Numerical modeling of Non-ideal Multicomponent mixture Sprays

Vaisakhan VS

A Dissertation Submitted to

Indian Institute of Technology Hyderabad

In Partial Fulfillment of the Requirements for

The Degree of Master of Technology

भारतीय प्रौद्योगिकी संस्थान हैदराबाद
Indian Institute of Technology Hyderabad

Department of Mechanical and Aerospace Engineering

July, 2014

Declaration

I declare that this written submission represents my ideas in my own words, and where others' ideas or words have been included, I have adequately cited and referenced the original sources. I also declare that I have adhered to all principles of academic honesty and integrity and have not misrepresented or fabricated or falsified any idea/data/fact/source in my submission. I understand that any violation of the above will be a cause for disciplinary action by the Institute and can also evoke penal action from the sources that have thus not been properly cited, or from whom proper permission has not been taken when needed.

_____

(Signature)

_____

(Vaisakhan VS)

_____

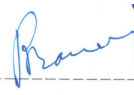(ME12M1028)

Approval Sheet

This thesis entitled Numerical modeling of Non-ideal Multicomponent mixture Sprays by Vaisakhan VS is approved for the degree of Master of Technology from IIT Hyderabad.

(Dr. K Venkatasubbaiah)Examiner

Dept. of Mechanical and Aerospace Engg.

IIT Hyderabad

(Dr. Saptarshi Majumdar)Examiner

Dept. of Chemical Engg.

IIT Hyderabad

(Dr. Raja Banerjee)Adviser

Dept. of Mechanical and Aerospace Engg.

IIT Hyderabad

iii

Acknowledgements

Dedicated to

Qube

Abstract

Modeling a multi-component fuel mixture had been of utmost importance in analyzing the atomization and evaporation characteristics, penetration length of the mixture and the distribution of mixture inside the engine chamber at different operating pressures, temperatures and the concentrations of the mixture. The present study is done on a heterogeneous mixture of iso-octane and ethanol to deduct the spray penetration at various cabin pressures and temperatures and the simulation results have been presented in the work. WAVE model have been activated as the secondary break-up model for the atomization of droplets. The droplets are continuously tracked for its properties using the discrete phase model and are coupled with the continuous phase for energy and momentum. The vapour-liquid equilibrium is established using the concentrations of the mixture and individual components with the help of user inputted C-code. The simulation result for a single component droplet of do-decane has been validated with the experimental results. A parametric study on the ideal multi-component mixture model has been done to show the variation in spray penetration length at temperatures 500,700 and 900 k with varying cabin pressures of 1.1, 3.0 and 5.0 Mpa. The ideal multi-component mixture shall be extended to non-ideal mixtures of hydrocarbon and alcohols.

Contents

Chapter 1

Introduction

Fuel injection is a system for admitting fuel into an internal combustion engine and has become the primary fuel delivery system used in automotive engines, having replaced carburetors during the 1980s and 1990s. A variety of injection systems have existed since the earliest usage of the internal combustion engine. The primary difference between carburetors and fuel injection is that fuel injection atomizes the fuel by forcibly pumping it through a small nozzle under high pressure, while a carburetor relies on suction created by intake air accelerated through a Venturi tube to draw the fuel into the airstream. Modern fuel injection systems are designed specifically for the type of fuel being used. Some systems are designed for multiple grades of fuel (using sensors to adapt the tuning for the fuel currently used). Most automotive fuel injection systems are for either gasoline or diesel applications.

1.1 Atomization of Sprays

The application and utilization of sprays is not new and in modern society it is extensive enough that almost every industry and household uses some form of sprays. The need to understand the physical structure of liquids under conditions of higher shear rates and interaction with gaseous flow is an increasing scientific interest in atomization.

A Spray is a dynamic collection of drops dispersed in a gas and a spray nozzle is a precision device that facilitates dispersion of liquid into a spray. Nozzles are used for three purposes: to distribute a liquid over an area, to increase liquid

surface area, and create impact force on a solid surface. A wide variety of spray nozzle applications use a number of spray characteristics to describe the spray. Spray nozzles can be categorized based on the energy input used to cause atomization, the breakup of the fluid into drops. Spray nozzles can have one or more outlets; a multiple outlet nozzle is known as a compound nozzle. Single-fluid or hydraulic spray nozzles utilize the kinetic energy of the liquid to break it up into droplets. This most widely used type of spray nozzle is more energy efficient at producing surface area than most other types. As the fluid pressure increases, the flow through the nozzle increases, and the drop size decreases. Many configurations of single fluid nozzles like Plain-orifice nozzle, Shaped-orifice nozzle, Surface-impingement nozzle, Pressure-swirl nozzle, Solid-cone nozzle, Compound nozzle are used depending on the spray characteristics desired. Another form of producing sprays is by Rotary Atomizers which use a high speed rotating disk, cup or wheel to discharge liquid at high speed to the perimeter, forming a hollow cone spray. The rotational speed controls the drop size. Commonly used Rotary Atomizers are Ultrasonic Atomizers and Electrostatic Atomizers.

Liquid Sprays are involved in many engineering applications in modern world which mainly include Fuel Sprays, Industrial Sprays and Sprays for Agricultural purposes. Industrial Sprays have displayed its potential in almost every fields like Electrical power generation, Manufacturing, Electronics, Steel industry, Chemical and pharmaceutical industry, Waste Treatment, Food and Beverages, Consumer products and so on. Fuel Sprays of hydrocarbon liquids (fossil fuels) are among the most economically significant applications of sprays. Examples include fuel injectors for Gasoline and Diesel engines, atomizers for jet engines (gas turbines), atomizers for injecting heavy fuel oil into combustion air in steam boiler injectors, and rocket engine injectors. Dispersion of the fuel into the combustion air is critical to maximize the efficiency of these systems and minimize emissions of

2

pollutants (soot, NOx, CO) leading to constant studies in Spray Models and Spray Calibration.

1.2 Sprays in IC Engine

Particulate and NOx emissions have been a profound problem in the near past due to the rising number of vehicles throughout the world. Consciousness in the environmental impact of the engine and the push of governments has led the automotive industry to spend considerable resources researching ways to improve engine emission and efficiency. The replacement of carburetor with port fuel injection laid a check on the amount of fuel injected for each cycle which can now be better controlled, leading to better fuel economy. At the same time, three way catalytic converters were introduced in order to reduce the amount of hydrocarbon (HC), carbon monoxide (CO) and nitric oxide (NOx) present in the exhaust gases [21]. These converters were designed in such a way that their efficiency was optimal with an engine running with a stoichiometric mixture. However, three way catalytic converters are very sensitive to the mixture air-to-fuel ratio and their efficiency degrades rapidly for any deviation from stoichiometric condition. The combination of port fuel injection and catalytic converters led to a significant decrease of emissions. Reduction in fuel consumption was also achieved by running the engine at less than stoichiometric air-to-fuel ratio, the lean-burn operation, under low-load or idle conditions. Though the port fuel injection system has some advantages, it cannot meet the increased demands of performance, emission legislation and fuel economy of the present day.

The electronic controlled Gasoline Direct Injection (GDI) engines gave a number of features, which could not be realized with port injected engines: avoiding fuel wall film in the manifold, improved accuracy of air/fuel ratio during dynamics, reducing throttling losses during gas exchange ; higher thermal efficiency by

3

stratified operation and increased compression ratio; decrease in the fuel consumption and CO2 emissions, lower heat losses, faster heating of the catalyst by injection during the gas expansion phase, increased performance and volumetric efficiency due to cooling of air charge, better cold start performance and better drive comfort.

To achieve higher fuel economy, concepts of homogeneous lean mode and stratified charge mode were studied and implemented in industry. However these modes need a better after treatment of the exhaust gases for removing emissions. To reduce fuel consumption and to be within the emission standards, new mixing techniques and spray calibration techniques are under constant study. Mixing techniques focus more on the engine-piston geometry, injection locations and valve timings. Spray calibration techniques include more of spray modeling aspects including the spray penetration, droplet evaporation and atomization. In this thesis, more importance have been laid on numerical modeling of the Multi-Component mixture (hydrocarbon-alcohol) sprays to study the effect of the parameters and the operating conditions on the spray characteristics like penetration depth, and molar concentrations of the components of the mixture.

1.3   Objectives

The principal objective of this work is to develop an evaporation model for Non-Ideal Multicomponent mixture spray of hydrocarbon and alcohol with customized User defined functions for various properties and for phase equilibrium during evaporation and to analyze the penetration length of the mixture spray at various proportions of hydrocarbon and alcohol.

1)   The first phase of this work is a simulation study on a single component droplet and to be validated with the experimental results [2].

4

2) The second phase of this study is to extend the above work to ideal multi-component mixture with user defined properties in a Lagrangian framework and analyze the spray penetration for a mixture of iso-octane and n-heptane under different cabin pressures (1.1, 3 and 5 Mpa) and temperatures (300,500,700 and 900K).

3) The third phase of the work is to move on to a non-ideal mixture of iso-octane and ethanol to analyze the spray characteristics numerically. In this part the vapor liquid equilibrium will be established by means of a User defined code and shall be compared with the existing scheme.

1.4   Thesis Structure

The structure of the thesis follows the above objectives with Chapter 1 giving a brief introduction about how sprays are created, their use in modern engineering applications and how developments in sprays and fuel injection had an effect on the IC engines over the years and a brief literature survey on the data and other parameters referred which helped me in this thesis and the objectives for this present work. Chapter 2 presents a detailed literature review on the behind mathematical formulations and CFD modeling of sprays which helps in understanding the physics of Discrete Phase model (Lagrangian frame of reference). .Chapter 3 will be detailing about the numerical setup of the work including the properties of all the materials used and the setting in the simulation software and Chapter 4 will contain the relevant results for the above objectives stated and their discussions followed by conclusions and references. Solver settings in chapter 3 and results and discussions in chapter 4 will essentially be divided into three parts as per mentioned in the objectives.

Chapter 2

Spray Modeling

The dynamics of Multiphase flows can now be well analyzed with advances in the computational fluid mechanics. There are two approaches for numerically modeling a multiphase flow, Euler-Euler approach and Euler-Lagrange approach. This research work is based on Euler-Lagrange approach using the discrete phase model to numerically model the particles of a spray. The following chapter will throw light on different injection models, concentrating on solid cone model used in this research work and moving onto the underlying physics of modeling a liquid spray laying emphasis on the primary and secondary breakup of spray, equations that define the flow of liquid, mainly mass, momentum and energy equations, both in the continuous phase and the discrete phase and how the above phases are coupled to get a solution. This chapter also indicates how the particles are being tracked for mass and other properties in a brief manner.

2.1 The Euler-Lagrange Approach

In Euler-Lagrange approach (discrete phase model), the fluid phase is treated as a continuum by solving the Navier-Stokes equations, while the dispersed phase is solved by tracking a large number of particles, bubbles, or droplets through the calculated flow field. The dispersed phase can exchange momentum, mass, and energy with the fluid phase by means of a coupling. A fundamental assumption made in this model is that the dispersed second phase occupies a low volume fraction, even though high mass loading ($\dot{m}_{particles} \geq \dot{m}_{fluid}$) is acceptable [24]. The particle or droplet trajectories are computed individually at specified intervals during the fluid phase calculation. This makes the model appropriate for the

6

modeling of spray dryers, coal and liquid fuel combustion, and some particle-laden flows, but inappropriate for the modeling of liquid-liquid mixtures where the volume fraction of the second phase cannot be neglected [24].

The discrete phase model cannot be used to model a continuum where particles are suspended for a long time and can be used when the particles are injected at a constant rate into a domain which has a well-defined entrance and exit with appropriate boundary conditions. The discrete phase model cannot be used with VOF models for modeling multiphase flows and numerical simulations involving parallel processing are not compatible with discrete phase model.

2.2   Particle motion theory

2.2.1 Particle force balance and equation of motion

The trajectory of a discrete phase particle or droplet can be predicted by integrating the force balance on a single droplet in a lagrangian reference frame [24]. The force balance equates the particle inertia with the forces acting on the particle and represented as follows,

$$\frac{du_p}{dt} = F_D\big(u - u_p\big) + \frac{g_x(\rho_p - \rho)}{\rho_p} + F_x \tag{2.1}$$

$$F_D = \frac{18\mu}{\rho_p d_p^2}\,\frac{C_D Re}{24} \tag{2.2}$$

$$Re \equiv \frac{\rho d_p(u_p - u)}{\mu} \tag{2.3}$$

where F_x is an additional acceleration term, $F_D\big(u - u_p\big)$ is the drag force per unit particle mass, Re is the relative Reynolds number, u is the fluid phase velocity, u_p is the particle velocity, μ is the molecular viscosity of the fluid, ρ is the fluid

density, ρ_p is the density of the particle, and d_p is the particle diameter. The coefficient of drag (C_D) is formulated from the spherical drag law,

$$C_D = a_1 + \frac{a_2}{Re} + \frac{a_3}{Re^2} \tag{2.4}$$

where a_1, a_2, and a_3 are constants that apply over several ranges of Re given by Morsi and Alexander [3].

Additional forces (F_x) are considered when a virtual mass force arise for accelerating the fluid around a particle or due to the force created by a pressure gradient. F_x also includes forces generated due to the rotation of a reference frame, Thermophoretic force , Brownian force or Saffman's lift force. However F_x is not considered in this research work.

The trajectory equations are solved by stepwise integration over discrete time steps. Integration of time in Equation 2.1 yields the velocity of the particle at each point along the trajectory, with the trajectory itself predicted by,

$$\frac{dx}{dt} = u_p \tag{2.5}$$

Equation 2.1 and 2.5 are a set of coupled ordinary differential equations and equation 2.1 can be modified as,

$$\frac{du_p}{dt} = \frac{1}{\tau_p}\left(u - u_p\right) + a \tag{2.6}$$

where the term $'a'$ includes accelerations due to all other forces except drag force. Equation 2.6 can be solved for a, τ_p and u by analytical discretization scheme for calculating the fluid and particle velocity field or by using a numerical discretization scheme like Euler implicit scheme or using a Runge-Kutta scheme published by Cash and Karp [4].

8

2.2.2   Turbulent Dispersion of particles

The dispersion of particles due to turbulence in the fluid phase can be predicted using the stochastic tracking model or the particle cloud model. The stochastic tracking (random walk) model includes the effect of instantaneous turbulent velocity fluctuations on the particle trajectories through the use of stochastic methods .The particle cloud model tracks the statistical evolution of a cloud of particles about a mean trajectory . The concentration of particles within the cloud is represented by a Gaussian probability density function (PDF) about the mean trajectory [24].

In the stochastic tracking approach, turbulent dispersion of particles is predicted by integrating the trajectory equations for individual particles, using the instantaneous fluid velocity, $\overline{u} + u'(t)$, along the particle path during the integration. The random effects of turbulence on the particle dispersion can be included by computing the trajectory in this manner for a sufficient number of representative particles. A stochastic method known as discrete random walk model is used to determine the instantaneous gas velocity. In the discrete random walk (DRW) model, the fluctuating velocity components are discrete piecewise constant functions of time [24]. Their random value is kept constant over an interval of time given by the characteristic lifetime of the eddies. The DRW model may give nonphysical results in strongly nonhomogeneous diffusion dominated flows, where small particles should become uniformly distributed. Instead, the DRW will show a tendency for such particles to concentrate in low-turbulence region of the flow. Prediction of particle dispersion makes use of the concept of the integral time scale, T, which describes the time spent in turbulent motion along the particle path, ds and is proportional to the particle dispersion rate.

$$T = \int_0^\infty \frac{u_p'(t)u_p'(t+s)}{\overline{u_p'^2}} \, ds \qquad (2.7)$$

In the discrete random walk (DRW) model, or "eddy lifetime" model, the interaction of a particle with a succession of discrete stylized fluid phase turbulent eddies is simulated. Each eddy is characterized by a Gaussian distributed random velocity fluctuation, u', v', and w' and a time scale , τ_e. The values of, u', v', and w' that prevail during the lifetime of the turbulent eddy are sampled by assuming that they obey a Gaussian probability distribution, so that

$$u' = \zeta \sqrt{\overline{u'^2}} \tag{2.8}$$

$$\sqrt{\overline{u'^2}} = \sqrt{\overline{v'^2}} = \sqrt{\overline{w'^2}} = \sqrt{2k/3} \tag{2.9}$$

where ζ is a normally distributed random number, and the remainder of the right-hand side of equation 2.8 is the local RMS value of the velocity fluctuations. If isotropy is assumed, the RMS fluctuating components for $k - \varepsilon$ and $k - \omega$ turbulence models can be expressed in terms of the turbulence kinetic energy (k) at each point in the flow [24].

Particle dispersion due to turbulent fluctuations can also be modeled with the particle cloud model. The turbulent dispersion of particles about a mean trajectory is calculated using statistical methods. The concentration of particles about the mean trajectory is represented by a Gaussian probability density function (PDF) whose variance is based on the degree of particle dispersion due to turbulent fluctuations [24]. The mean trajectory is obtained by solving the ensemble averaged equations of motion for all particles represented by the cloud. The cloud enters the domain either as a point source or with an initial diameter. The cloud expands due to turbulent dispersion as it is transported through the domain until it exits. The distribution of particles in the cloud is defined by a probability density function (PDF) based on the position in the cloud relative to the cloud center. The value of the PDF represents the probability of finding particles represented by that cloud with residence time t at location x_i in the flow field. The average particle number

density can be obtained by weighting the total flow rate of particles represented by that cloud, $\dot{m}$,

$$\langle n(x_i) \rangle = \dot{m}\, P(x_i, t) \tag{2.10}$$

$$P(x_i, t) = \frac{1}{(2\pi)^{3/2} \prod_{i=1}^{3} \sigma_i}\, e^{-s/2} \tag{2.11}$$

where

$$s = \sum_{i=1}^{3} \left(\frac{x_i - \mu_i}{\sigma_i} \right)^2 \tag{2.12}$$

The mean of the PDF or the center of the cloud, at a given time represents the most likely location of the particles in the cloud. The radius of the particle cloud is based on the variance, $\sigma_i^2(t)$, of the PDF. The mean location is obtained by integrating a particle velocity as defined by an equation of motion for the cloud of particles and the variance of the PDF can be expressed in terms of two particle turbulence statistical quantities,

$$\mu_i(t) \equiv \langle x_i(t) \rangle = \int_0^t \langle V_i(t_1) \rangle dt_1 + \langle x_i(0) \rangle \tag{2.13}$$

$$\sigma_i^2(t) = 2 \int_0^t \langle u_{p,i}'^2(t_2) \rangle dt_1 \int_0^{t_2} R_{p,ii}(t_2, t_1) dt_1 dt_2 \tag{2.14}$$

where $\langle u_{p,i}'^2 \rangle$ are the mean square velocity fluctuations, and $R_{p,ii}(t_2, t_1)$ is the particle velocity correlation function,

$$R_{p,ii}(t_2, t_1) = \frac{\langle u_{p,i}'(t_2) u_{p,j}'(t_1) \rangle}{\left[\langle u_{p,i}'^2(t_2) u_{p,j}'^2(t_1) \rangle \right]^{1/2}} \tag{2.15}$$

11

2.3   Laws of Heat and Mass exchange

The reacting particles or droplets can be modeled and their impact on the continuous phase can be examined by discrete phase modeling by activating certain physical models and heat transfer relationship, also termed as laws. Different laws are deployed depending on the type of particle in the domain and explained below. Table 2.1 shows the laws activated for different particle types [24].

Table 2.1: laws activated for different particle types

Particle type	Description	Laws activated
Inert	Inert/ heating or cooling	1,6
Droplet	Heating /evaporation/boiling	1,2,3,6
Multicomponent	Multi-component droplets/particles	7

2.3.1   Inert heating or cooling law

The inert heating or cooling laws (Laws 1 and 6) are applied when the particle temperature is less than the vaporization temperature, T_{vap}, and after the volatile fraction, $f_{v,0}$, of a particle has been consumed.

Law 1: $$T_p < T_{\text{vap}} \qquad\qquad 2.16$$

Law 6: $$m_p \leq (1 - f_{v,0})m_{p,0} \qquad\qquad 2.17$$

where T_p is the particle temperature, $m_{p,0}$ is the initial mass and m_p is the current mass of the particle.

Law 1 will be applied until the temperature of the particle/ droplet reaches the vaporization temperature and returning to law 6 when the volatile portion of the particle/droplet has been consumed. The vaporization temperature, T_{vap}, in only a arbitrary constant for the onset of vaporization. Law 1 or law 6 assumes a

simple heat balance to relate particle temperature, T_p, to the convective and absorption or emission of radiation to or from the surface [24],

$$m_p c_p \frac{dT_p}{dt} = hA_p\left(T_\infty - T_p\right) + \epsilon_p A_p \sigma(\theta_R^4 - T_p^4) \tag{2.18}$$

where,

m_p = mass of the particle (kg)

c_p = heat capacity of the particle (J/ kg-K)

A_p = surface area of particle (m^2)

T_∞ = local temperature of continuous phase (K)

h = convective heat transfer coefficient (W/ m^2-K)

ϵ_p = particle emissivity (dimensionless)

σ = Stefan-Boltzmann constant (5.67×10^{-8} W/m^2-K^4)

θ_R = radiation temperature

The heat transfer coefficient h is evaluated using Ranz and Marshall correlation [4,5],

$$Nu = \frac{hd_p}{k_\infty} = 2.0 + 0.6\, Re_d^{1/2} Pr^{1/3} \tag{2.19}$$

where,

d_p = particle diameter (m)

k_∞ = thermal conductivity of continuous phase (W/m-K)

Re_d = relative Reynold's number based on particle diameter

Pr = Prandtl number of the continuous phase

The second part, radiation interaction, of equation 2.18 is valid only when the particle radiation interaction in DPM model is turned on. The above equation is

integrated to obtain the particle temperature as soon as the particle trajectory is computed. During Laws 1 and 6, particles/droplets do not exchange mass with the continuous phase and do not participate in any chemical reaction.

2.3.2 Droplet Vaporization law

Droplet vaporization law (law 2) is applied to predict the vaporization from a discrete phase droplet. This law is initiated when the temperature of the droplet reaches the vaporization temperature, T_{vap}, and continues until the droplet reaches the boiling point, T_{bp}, or until the droplet's volatile fraction is completely consumed.

$$T_{\text{vap}} \leq T_p < T_{\text{bp}} \tag{2.20}$$

$$m_p > (1 - f_{v,0})m_{p,0} \tag{2.21}$$

The rate of vaporization is governed by gradient diffusion, with the flux of droplet vapor into the liquid phase related to the difference in vapor concentration at the droplet surface and the bulk gas [24],

$$N_i = k_c(C_{i,s} - C_{i,\infty}) \tag{2.22}$$

where,

N_i = molar flux of vapor (kgmol/m^2-s)

k_c = mass transfer coefficient (m/s)

$C_{i,s}$ = vapor concentration at droplet surface (kgmol/m^3)

$C_{i,\infty}$ = vapor concentration in the bulk gas (kgmol/m^3)

The mass transfer coefficient in Equation 2.22 is calculated from the Sherwood number correlation [4,5],

$$Sh_{AB} = \frac{k_c d_p}{D_{i,m}} = 2.0 + 0.6 \, Re_d^{1/2} Sc^{1/3} \tag{2.23}$$

where,

d_p = particle diameter (m)

$D_{i,m}$ = Diffusion coefficient of vapor in the bulk (m^2/s)

Sc = Schmidt number

The concentration of vapor at the droplet surface is evaluated by assuming that the partial pressure of vapor at the interface is equal to the saturated vapor pressure, p_{sat}, at the particle droplet temperature, T_p, and the concentration of vapor in the bulk gas is known from solution of the transport equation for species i.

$$C_{i,s} = \frac{p_{sat}(T_p)}{RT_p} \tag{2.24}$$

$$C_{i,\infty} = X_i \, \frac{p}{RT_\infty} \tag{2.25}$$

where X_i is the local mole fraction of species i, p is the local absolute pressure, T_∞ is the local bulk temperature in the gas and R is the universal gas constant. The heat transfer to the droplet is same as equation 2.18 with the addition of a latent heat transfer between the droplet and continuous phase.

2.3.3 Multicomponent particle law

Multicomponent particles are defined as a mixture of different species within droplets. The particle mass m is the sum of the masses of the components. The density of the particle ρ_p can be either constant or volume-averaged.

$$m = \sum_i m_i \tag{2.26}$$

$$\rho_p = \left(\sum_i \frac{m_i}{m\rho_i} \right)^{-1} \tag{2.27}$$

For particles containing more than one component, it is difficult to assign the whole particle to one process like boiling or heating. Therefore it must be modeled by integrating all processes of relevance in one equation. Equation 2.28 and 2.29 shows the temperature and mass transfer as sum of the sources from the partial processes.

$$m_p c_p \frac{dT_p}{dt} = hA_p(T_\infty - T_p) + \epsilon_p A_p \sigma(\theta_R^4 - T_p^4) + \sum_i \frac{dm_i}{dt}(h_{i,p} - h_{i,g}) \tag{2.28}$$

$$\left(\frac{dm_i}{dt} \right) = A_p M_{w,i} k_{c,i}(C_{i,s} - C_{i,\infty}) \tag{2.29}$$

where $M_{w,i}$ is the molecular weight of species i, $k_{c,i}$ is the mass transfer coefficient of component I calculated from Sherwood relation.

The concentration of vapor at the particle surface $C_{i,s}$ depends upon the saturation pressure of the component. Compressibility, Z_V, is taken into account and $C_{i,s}$ is calculated according to Peng-Robinson real gas model represented in equation 2.30

$$C_{i,s} = x_i^V \frac{p}{Z_V RT} \tag{2.30}$$

where x_i^V is the vapor mole-fraction of the species i, p is the operating pressure and T is the operating temperature.

2.4   Vapor-Liquid Equilibrium theory

The rate at which a species is transferred from one phase to the other depends on the departure of the system from equilibrium. Vapor-liquid equilibrium (VLE) relationships in multicomponent systems are needed for computation of evaporation rates in spray combustion problems. The rate of evaporation of N components from the surface of a single droplet can also be determined from the mass transfer equation 2.22 replacing p_{sat} with p_i, partial pressure of species i. The partial pressure of species i can be obtained from the general expression for two phase equilibrium, equating the fugacity of the liquid and vapor mixture components. However, under low pressure conditions the gas and liquid phase can be considered to be ideal, it reduces to Raoult's law expressed as [24],

$$x_i^V p = x_i^L \, p_{sat,i} \tag{2.31}$$

Equation 2.30 which gives concentration of vapor from a particle surface, according to Peng-Robinson real gas model, it can be modified as,

$$C_{i,s} = x_i^L \frac{p_{sat,i}}{Z_V RT} \tag{2.32}$$

At high pressure conditions real gas nature need to be considered and therefore Peng-Robinson equation of state must be used and compressibility, Z_V, can represented as follows [24].

$$Z_V = \frac{V}{V-b} - \frac{aV/RT}{V^2 + 2bV - b^2} \tag{2.33}$$

where a and b are determined by the composition using a simple mixing law,

$$a = \sum_{i=1}^{N} \sum_{j=1}^{N} x_i x_j \sqrt{a_i a_j} \tag{2.34}$$

$$b = \sum_{i=1}^{N} x_i b_i \tag{2.35}$$

where N is the number of components in the mixture and a_i and b_i can be calculated as [23]:

$$a_i = \left(0.45724 \frac{R^2 T_{c,i}^2}{P_{c,i}} \right) \left[1 + (0.37464 + 1.54226\omega_i - 0.2699\omega_i^2)(1 - \left(\frac{T}{T_{c,i}} \right)^{1/2} \right]^2 \tag{2.36}$$

$$b_i = 0.0778 \frac{RT_{c,i}}{P_{c,i}} \tag{2.37}$$

where $T_{c,i}$ is the critical temperature, $P_{c,i}$ is the critical pressure and ω_i is the accentric factor of the component i.

2.5   Break-up Phenomena in Sprays

2.5.1   Break-up regimes

Dependent on the relative velocity and the properties of the liquid and surrounding gas, the breakup of a liquid jet is governed by different break-up mechanisms. These different mechanisms are usually characterized by break-up length, the distance between the nozzle and the point of first droplet formation, and the size of the droplets that are produced. Figure 2.1 and 2.2 shows the schematic of a liquid spray an schematic of blobs from a liquid jet during fuel injection [7]

18
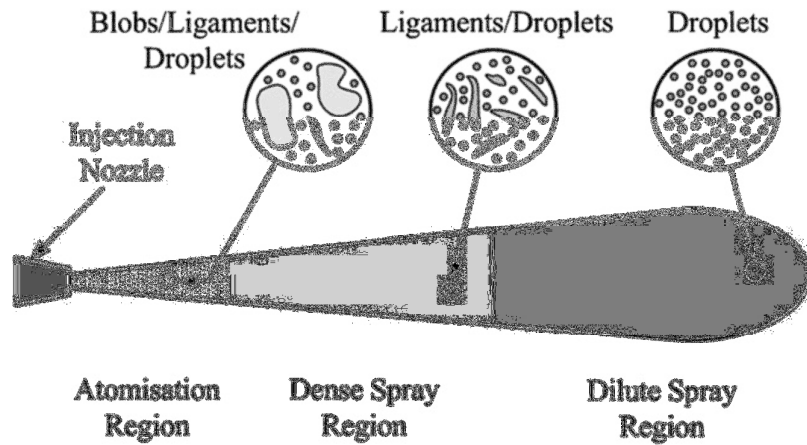
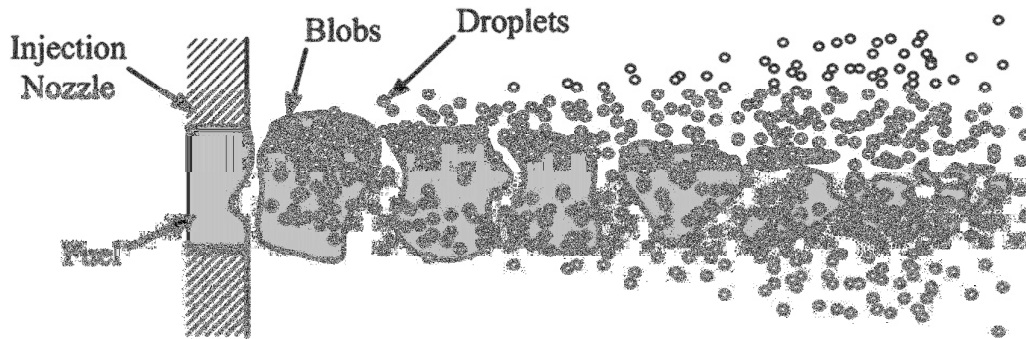**Fig-2.1: Schematic of a liquid spray [7]**

Fig-2.2: Schematic of blobs emanating from liquid jet in an injection [7]

The drop break-up in a spray is caused by aerodynamic forces (friction and pressure) induced by the relative velocity u_{rel} between droplet and surrounding gas. The aerodynamic forces result in an unsteady growing of waves on the gas/liquid interface or of the whole droplet itself, which finally leads to disintegration and to the formation of smaller droplets. These droplets are again subject to further aerodynamically induced break-up. The surface tension force on the other hand tries to keep the droplet spherical and counteracts the deformation force. The surface tension force depends on the curvature of the surface: the smaller the droplet, the

19

bigger the surface tension force and the bigger the critical relative velocity, which leads to an unsteady droplet deformation and to disintegration [21]. This behavior is expressed by the gas phase Weber number,

$$We_g = \frac{U^2 \, d \, \rho_g}{\sigma} \tag{2.38}$$

where d is the droplet diameter before break-up, σ is the surface tension between liquid and gas, u_{rel} is the relative velocity between droplet and gas, and ρ_g is the gas density. Fig 2.3 shows the break up regimes of drops according to Wierzba [8].
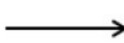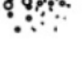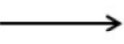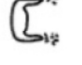
Vibrational break-up	⟶	◯	8	◦ ◦	
Bag break-up	⟶	◯〇	◻	◻	⋰⋰
(Bag-streamer) break-up	⟶	◯〇	◻	◻	⋰⋰
Stripping break-up	⟶	◯	⊂	⊂	⊂
Catastrophic break-up	⟶	◯	⦿	⦿	⦿

Fig-2.3: Drop Break-up regimes according to Wierzba [8]

2.5.2   Primary Break-up

The primary break-up process provides the starting conditions for the calculation of the subsequent mixture formation inside the cylinder, such as initial radius and velocity components (spray angle), which are mainly influenced by the flow conditions inside the nozzle holes. The simplest and most popular way of defining the starting conditions of the first droplets at the nozzle hole exit of full-cone

Gasoline sprays is the blob method developed by Reitz and Diwakar [9]. The blob method is based on the assumption that atomization and drop break-up within the dense spray near the nozzle are indistinguishable processes, and that a detailed simulation can be replaced by the injection of big spherical droplets with uniform size, which are then subject to secondary aerodynamic-induced break-up. The diameter of these blobs equals the nozzle hole diameter D (mono-disperse injection) and the number of drops injected per unit time is determined from the mass flow rate. Although the blobs break up due to their interaction with the gas, there is a region of large discrete liquid particles near the nozzle, which is conceptually equivalent to a dense core. Fig 2.4 shows a typical blob method break-up [9].
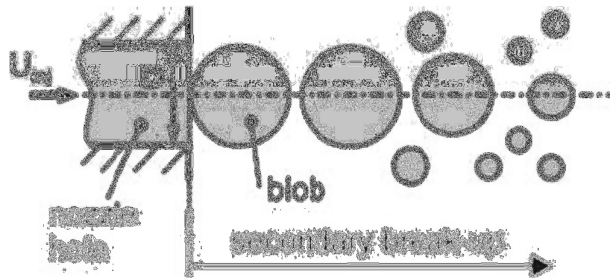
Fig-2.4: Blob generation and break-up [9]

The blob method is a simple and well-known method of treating the primary break-up in Eulerian-Lagrangian CFD codes. As far as there is no detailed information about the composition of the primary spray, and measurements about the spray cone angle are available, it is the best way to define the initial starting conditions for the liquid entering the chamber. In this research, defaut primary break-up models are assumed and no further explorations on primary break-ups have been done. The initial spray angle is specified from the experimental results [2].

2.5.3 Secondary Break-up

The most widely used secondary break-up models for the numerical simulation purposes are Taylor analogy break-up (TAB) model and Kevin-Helmoltz(KH) or Wave model. Wave model is recommended for high speed injections and injections with higher weber number. In this research work, Wave model has been selected as the secondary break-up model. Fig 2.5 show different types of secondary break-up of droplets in TAB and KH models [22].
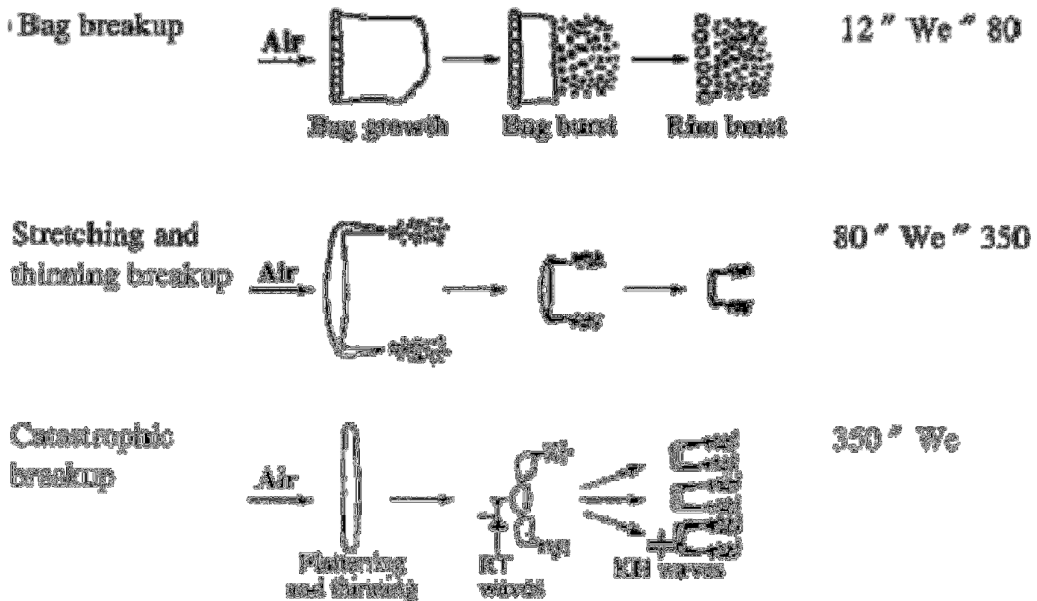
Fig-2.5: Secondary droplet atomization [22]

Wave model was proposed by Reitz [9] and considers the breakup of the droplets to be induced by the relative velocity between the gas and liquid phases and assumes that the time of breakup and the resulting droplet size are related to the fastest-growing Kelvin-Helmholtz instability. The wavelength and growth rate of this instability are used to predict details of the newly formed droplets. The model is based on a first order linear analysis of a Kelvin-Helmholtz instability growing on the surface of a cylindrical liquid jet with initial radius, a, that is penetrating into a

stationary incompressible gas with a relative velocity, u_{rel} . Both the liquid and the gas are assumed to be incompressible, and the gas is assumed to be inviscid. Furthermore, it is assumed that due to the turbulence generated inside the nozzle hole the jet surface is covered with a spectrum of sinusoidal surface waves with an infinitesimal axisymmetric displacement, $\eta = \eta_0 e^{\Omega t}$ ($\eta \ll r$), causing small axisymmetric fluctuating pressures as well as axial and radial velocity components in both liquid and gas. These surface waves grow because of aerodynamic forces due to the relative velocity between liquid and gas (shear flow waves). Fig 2.6 shows the surface wave generation and a blob break-up [7].
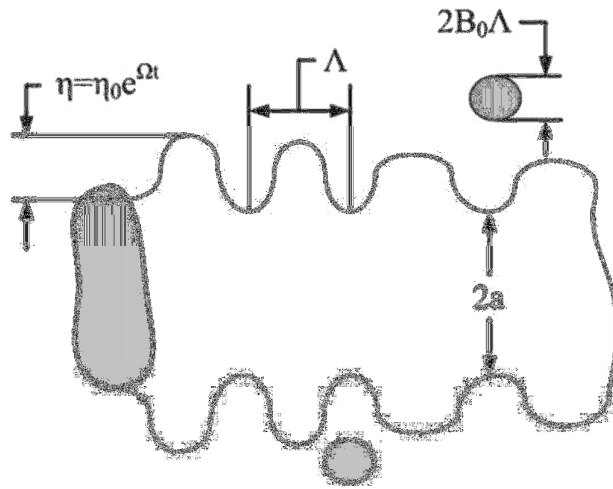
Fig-2.6: Schematic showing the surface wave generation [7]

The motion of liquid and gas are described by the linearized Navier-Stokes equations for both phases. The solution is found by transforming the equations of motion into stream and potential functions. Reitz and Bracco [10] yielded a dispersion equation relating the growth rate, Ω , of a perturbation to its wavelength: $\Lambda = 2\pi/k$ and for a most unstable surface wave, growth rate and the corresponding wavelength are given by Equation 2.39 and 2.40 [9].

23

$$\Omega \left[\frac{\rho_l a^3}{\sigma} \right]^{0.5} = \frac{0.34 + 0.38 We_g^{1.5}}{(1 + Z)(1 + 1.4T^{0.6})} \tag{2.39}$$

$$\frac{\Lambda}{a} = 9.02 \frac{(1 + 0.45Z^{0.5})(1 + 0.4T^{0.7})}{\left(1 + 0.87 We_g^{1.67}\right)^{0.6}} \tag{2.40}$$

$$Z = \frac{\sqrt{We_l}}{Re_l} \qquad T = Z\sqrt{We_g} \qquad We_g = \frac{\rho_g a u_{rel}^2}{\sigma} \qquad We_l = \frac{\rho_l a u_{rel}^2}{\sigma}$$

where T and Z are Taylor number and Ohnesorge number respectively, a is the radius of the undisturbed jet. Waves grow on the drop surface with growth rate Ω and wavelength, Λ. New child drops are formed from the surface waves that are sheared off the parent drops, and assumed that the radius of the new droplets, r is proportional to the wavelength,

$$r = B_0 \Lambda \tag{2.41}$$

where $B_0 = 0.61$(a constant) and rate of change of droplet radius in parent parcel is given as,

$$\frac{da}{dt} = -\frac{(a - r)}{\tau}, r \leq a \tag{2.42}$$

where break-up time, τ, is given by,

$$\tau = \frac{3.726\, B_1 a}{\Lambda\Omega} \tag{2.43}$$

B_1 is another constant which can be varied from 1 to 60 and it decides the rate of breaking up of the droplets which in turn changes the penetration depth of the spray.

24

2.6   Coupling between discrete and continuous phase

The simulation software (ANSYS FLUENT) computes the trajectory of the particle and keeps track of the heat, mass, and momentum gained or lost by the particle stream that follows that trajectory and these quantities are incorporated in the subsequent continuous phase calculations. Thus, while the continuous phase always impacts the discrete phase, the effect of the discrete phase trajectories will have an impact on the continuum. This two-way coupling is accomplished by alternately solving the discrete and continuous phase equations until the solutions in both phases have stopped changing or convergence is achieved [24]. The interphase exchange of heat, mass, and momentum from the particle to the continuous phase is depicted qualitatively in Figure 2.7.
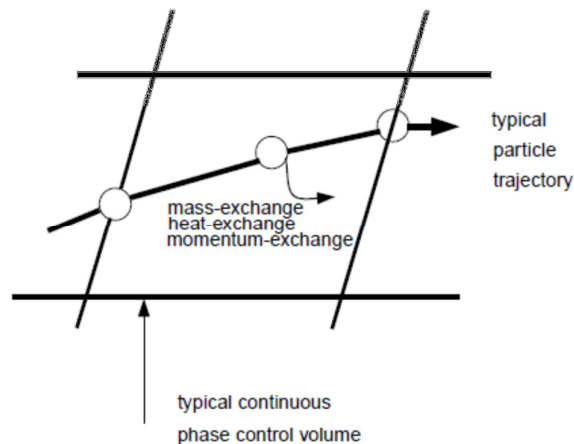
Fig-2.7: Mass, Momentum and heat exchange from the particle to continuous phase

2.6.1   Mass Exchange

The mass transfer from the discrete phase to the continuous phase is computed in ANSYS FLUENT by examining the change in mass of a particle as it passes through each control volume in the model. The mass exchange is calculated as in Equation 2.44 [24],

$$M = \frac{\Delta m_p}{m_{p,0}} \, \dot{m}_{p,0} \tag{2.44}$$

This mass exchange appears as a source of mass in the continuous phase continuity equation and as a source of a chemical species defined by you. The mass sources are included in any subsequent calculations of the continuous phase flow field

2.6.2 Momentum Exchange

The momentum transfer from the continuous phase to the discrete phase is computed in ANSYS FLUENT by examining the change in momentum of a particle as it passes through each control volume in the model. The momentum exchange is given by Equation 2.45 [24],

$$F = \sum \left(\frac{18\mu C_D Re}{24\rho_p d_p^2} (u_p - u) + F_{other} \right) \dot{m}_p \, \Delta t \tag{2.45}$$

where

μ = viscosity of fluid (kg/m-s)

ρ_p = density of particle (kg/m^3)

d_p = diameter of particle (m)

u_p = velocity of particle (m/s)

$\dot{m}_p$ = mass flow rate of the particles (kg/s)

u = velocity of fluid (m/s)

Δt = time step (s)

Re = Reynold's number

C_D = drag coefficient

F_{other} = other interaction forces

This momentum exchange appears as a momentum source in the continuous phase momentum balance in any subsequent calculations of the continuous phase flow field.

2.6.3 Heat Exchange

The heat transfer from the continuous phase to the discrete phase is computed in ANSYS FLUENT by examining the change in thermal energy of a particle as it passes through each control volume in the model. In the absence of a chemical reaction the heat exchange is given by Equation 2.46 [24],

$$Q = \frac{\dot{m}_{p,0}}{m_{p,0}}\left[\left(m_{p_{in}} - m_{p_{out}}\right)\left(-H_{lat_{ref}} + H_{pyrol}\right) - m_{p_{out}}\int_{T_{ref}}^{T_{p_{out}}} c_{p_p}dt + m_{p_{in}}\int_{T_{ref}}^{T_{p_{in}}} c_{p_p}dt\right]$$

(2.46)

where,

$\dot{m}_{p,0}$ = initial mass flow rate of the particle injection (kg/s)

$m_{p,0}$ = initial mass of the particle (kg)

$m_{p_{in}}$ = mass of the particle on cell entry (kg)

$m_{p_{out}}$ = mass of the particle on cell exit (kg)

c_{p_p} = heat capacity of the particle (J/kg-K)

$T_{p_{in}}$ = temperature of particle on cell entry (K)

$T_{p_{out}}$ = temperature of particle on cell exit (K)

T_{ref} = reference temperature for enthalpy (K)

H_{pyrol} = heat of pyrolysis as volatiles are evolved (J/kg)

$H_{lat_{ref}}$= latent heat at reference conditions (J/kg)

and $H_{lat_{ref}}$ is expressed as,

$$H_{lat_{ref}} = H_{lat} - \int_{T_{ref}}^{T_{bp}} c_{p_g}dt + \int_{T_{ref}}^{T_{bp}} c_{p_p}dt$$

(2.47)

where

c_{p_g} = heat capacity of gas product species (J/kg-K)

T_{bp} = boiling point temperature (K)

H_{lat} = latent heat at the boiling point temperature (J/kg)

27

Chapter 3

Solver Settings

In this study, spray and atomization of the inert and the multicomponent droplets is modeled in ANSYS FLUENT. This chapter details the pre-processing and the solver settings in FLUENT for all the three portions of this work i.e. inert droplet validation, ideal and non-ideal multicomponent study. This chapter provides information on the various mesh used for simulations, tabulates the properties of all the materials used in this work and formulates the details of the different User Defined Functions (UDF) written for calculating the various properties such as density, viscosity and vapor pressure. All the simulations were performed using Pressure based transient solver and the body force due to gravity was neglected.

3.1   Pre-processor settings

3.1.1   Mesh Setup

In this study, two grid sizes were evaluated, 1mm and 0.8mm, for grid sensitivity analysis using inert do-decane droplets. For evaporation cases, an extended mesh was used so that the droplets have sufficient time to get fully evaporated. The simulations were performed on a sector mesh containing an inlet, outlet and top wall. A periodic boundary condition was applied to the side surfaces of the sector. The specification of the meshes is listed in Table 3.1 and mesh for multicomponent simulation study is shown in Fig 3.1.

Table 3.1: Specifications of the different meshes

Specifications	Mesh-1	Mesh-2	Mesh-3
Size of mesh	1mm	0.8mm	1mm
Number of elements	28K	91K	152K
Length of mesh	100 mm	100mm	300mm
Sector angle	30 degree	30 degree	30 degree
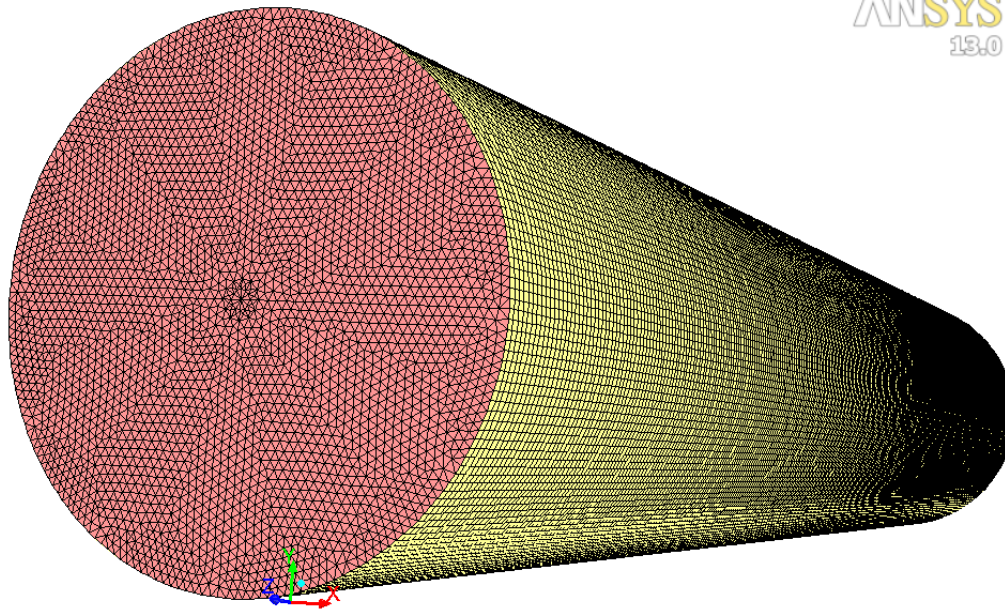
Fig-3.1: Cylindrical mesh for multicomponent simulation studies

3.1.2 Model setup

Model setup gives a detailed description of the models activated for each study, the values of the parameters in each model and the details of the injections defined. All the above will be recorded for the three case studies: Inert case, ideal multicomponent case and non-ideal multicomponent case with injection properties defined for three different inert case validations. Table 3.2 specifies the models activated for the three case studies.

Table 3.2: Models activated for different cases

Models	Inert	Ideal multicomp	Non-Ideal multicomp
Multiphase	OFF	OFF	OFF
Energy	OFF	ON	ON
Viscous	ON	ON	ON
Radiation	OFF	OFF	OFF
Species	OFF	ON	ON
Discrete phase	ON	ON	ON

Multiphase VOF models are not activated for any studies in this work and the sole focus was on Discrete phase modeling (DPM). Since the radiation model is not enabled the radiation part of the heat transfer in equations 2.18 and 2.28 was not activated. The model parameters and their values for viscous and species model for the various cases are explained below and Table 3.3 gives the parameters for the DPM model for the three cases of study.

- **Viscous model**: Standard $k - \epsilon$ (2 eqn) model with standard wall functions and the values of all the constants set to default for all the three cases.

- **Species model**: Species transport is disabled for inert case and enabled for ideal and non-ideal multicomponent case with "diffusion energy source" enabled and the number of volumetric species set to 3.

- **Energy Model**: Energy Model is disabled for inert case and is enabled for both ideal and non-ideal multicomponent cases

Table 3.3: DPM parameters for different cases

DPM Parameters	Inert	Ideal Multicomp	Non-ideal Multicomp
Drag law	Spherical	Spherical	Spherical
Droplet Collision	Enabled	Enabled	Enabled
Break-up model	Wave	Wave	Wave
B0	0.61	0.61	0.61
B1	Varies	60	20
Fluid flow time step	1e-03	1e-03	1e-03
Others	Default	Default	Default

For this study, only one injection is defined and the analysis was done for three inert droplet cases with different injection parameters. Injection parameters for the three inert validation cases are tabulated in Table 3.4. The operating conditions in the chamber /domain were varied for the three cases and are listed in Table 3.5.

Table 3.4: Injection parameters for inert validation cases

Injection Parameters	Case-1	Case-2	Case-3
Droplet diameter	0.3 mm	0.3mm	0.3mm
Injection velocity	102 m/s	90 m/s	86m/s
Particle Mass flow rate	6.05 g/s	5.36 g/s	5.13 g/s
Initial spray angle	7.5 deg	12.4 deg	16 deg

Table 3.5: Operating/chamber conditions for inert validation cases

Operating conditions	Case-1	Case-2	Case -3
Gas Temperature	300 K	300 K	300 K
Gas/Chamber Pressure	1.1 Mpa	3.0 Mpa	5.0 Mpa

The general injection properties like number of particle streams, type of primary breakup, type of diameter distribution and turbulent dispersion model for the 3 cases of study, inert, ideal and non-ideal multicomponent, are listed in Table 3.6.

Table 3.6: Injection properties for different cases

Injection Properties	Inert	Ideal Multicomp	Non-ideal Multicomp
Injection type	Solid cone	Solid cone	Solid cone
No: of particle streams	20	20	20
Particle type	Inert	Multicomponent	Multicomponent
Material	Do-decane	Gas-mixture	Gas-mixture
Diameter distribution	Uniform	Uniform	Uniform
Turbulent dispersion	DRW	DRW	DRW

- DRW- Discrete Random Walk Model (refer 2.2.2)

3.1.3 Materials

The inert study has been done on a do-decane droplet, the ideal multicomponent study on a mixture of iso-octane and nheptane and non-ideal study on a mixture iso-octane and ethanol. The mixture of iso-octane and nheptane were chosen as the ideal mixture because the vapor pressure of their solution obeys raoult's law and the activity coefficient of the components is equal to one. A mixture of iso-octane and ethanol is chosen for non-ideal mixture as their solution doesn't obey raoult's aw and activity coefficients of the components is not equal to one and calculated in this study. Iso-octane is the reference for octane rating of a fuel and ethanol has a high octane number and the evaporation rate for the mixture was enhanced by the addition of ethanol. Material properties for the components were obtained from given standard values [1, 23, 25]. Some properties like

saturation vapor pressure were defined by means of UDF's. The material properties for the various components used in this study are listed in Table 3.7.

Table 3.7: Material Properties for different components

Properties	Do-decane	Iso-octane	nheptane	Ethanol	Air
Molecular Weight	170.33	114.231	100.202	46.069	28.8
Critical Temperature	NA	543.90	540.2	513.92	131.96
Critical Pressure	NA	2.57e+06	2.74e+06	6.148e+06	3.74e+06
Accentric factor	NA	0.304	0.3495	0.649	0.0
Vapor Density	NA	4.84	4.25	2.06	varies
Vapor Thermal conductivity	NA	0.0117	0.0178	0.0145	0.0242
Vapor viscosity	NA	5.9303e-06	7e-06	1.08e-05	1.789e-05
Vapor C_p	NA	Polynomial	Polynomial	Polynomial	1006.43
Liquid density	840	695.5	684	813	0.0
Liquid Thermal conductivity	0.140	0.0995	0.140	0.182	0.0
Liquid viscosity	0.001315	0.000455	0.000409	0.0001233	0.0
Liquid C_p	NA	2037	2219	2470	0.0
Vaporization Temperature	NA	170	182.59	164	0.0
Boiling point	NA	398.82	371.57	351	0.0
Droplet Surface tension	NA	0.02	0.0198	0.0223	0.0

- NA- The property value was not relevant for this study
- C_p – Specific Heat Capacity (J/kg-K)

The units for the above properties are listed below:

Molecular weight- kg/kmol; Temperature- K; Pressure- Pa-s; Density $-kg/m^3$

Thermal conductivity- W/m-K; Viscosity- kg/m-s; Surface tension- N/m

3.1.4   Boundary Conditions

The sector mesh/domain typically contains an inlet, outlet, top wall and side surfaces which were assigned appropriate boundary conditions as listed in Table 3.8:

Table 3.8: Domain parts and their boundary conditions

Domain Part	Boundary condition	Discrete phase boundary condition
Inlet	Wall	Reflect
Outlet	Pressure-outlet	Reflect
Top-wall	Wall	Reflect
Side-wall	Periodic - Rotational	-
Interior	Interior	-

In pressure outlet boundary condition,

- Gauge pressure was set to zero
- Backflow Turbulent Kinetic energy and Turbulent Dissipation rate are assumed to be default values
- Backflow temperature set as 300 K (default)

In wall boundary condition,

- Stationary wall with No-slip shear condition
- Thermal boundary conditions set as default
- Species boundary condition – Zero Diffusive Flux for all the species

3.1.5 Customized Material Properties

User Defined Functions were written in C-code for properties like mixture density, thermal conductivity, and viscosity and for liquid properties like saturation vapor pressure. Vapor specific heat was inputted by means of a polynomial.

- Density of gas mixture: Density of the gas mixture was calculated by a UDF which accounts for the compressibility and mathematically formulated using Equation 2.33

- Viscosity : Wilke's Method has been used to determine the viscosity of the mixture [1,23], and is expressed as,

$$\mu_m = \sum_{i=1}^{N} \frac{x_i \mu_i}{\sum_{j=1}^{N} x_j \phi_{ij}}$$
(2.48)

where,

$$\phi_{ij} = \frac{\left[1 + \left(\mu_i/\mu_j\right)^{1/2} \left(M_j/M_i\right)^{1/4}\right]^2}{\left[8\left(1 + M_i/M_j\right)\right]^{1/2}}$$
(2.49)

where,

μ_m = viscosity of mixture (kg/m-s)

μ_i, μ_j = viscosities of the corresponding species (kg/m-s)

x_i, x_j = mole fractions of the corresponding species

M_i, M_j = Molecular weights of the corresponding species (kg/kmol)

- Thermal conductivity: Thermal conductivity was determined from Wassiljewa equation, including a factor by Mason and Saxena [23]

$$\lambda_m = \sum_{i=1}^{N} \frac{x_i \lambda_i}{\sum_{j=1}^{N} x_j A_{ij}}$$
(2.50)

where,

$$A_{ij} = \frac{\varepsilon \left[1 + \left(\lambda_i/\lambda_j\right)^{1/2}\left(M_j/M_i\right)^{1/4}\right]^2}{\left[8\left(1 + M_i/M_j\right)\right]^{1/2}}, \varepsilon = 1.065 \qquad (2.51)$$

where,

λ_m = Thermal conductivity of mixture (W/m-K)

λ_i, λ_j =Thermal conductivities of corresponding species (W/m-K)

x_i, x_j = mole fractions of the corresponding species

M_i, M_j = Molecular weights of the corresponding species (kg/kmol)

- Vapor Pressure: Saturation vapor pressure for the components was determined from the modified Antoine equation[23]

$$P_{vp\,mod} = \lambda_a e^{\left(A - \frac{B}{T_p + C - 273.15}\right)} \qquad (2.52)$$

where,

$P_{vp\,mod}$ = Modified vapor pressure (bar)

λ_a = Activity Coefficient calculated from UNIFAC method [23]

A, B   = Antoine Coefficients [23]

T_p = Particle Temperature (K)

3.2 Solution setup

The solution was run for time steps of 1e-04, 1e-05 and 1e-06 for time sensitivity study in inert validation case. Time-step 1e-05 was assumed for multicomponent parametric studies.

3.2.1 Solution Methods

SIMPLEC Scheme was selected for Pressure –velocity coupling with default skewness correction value. The Spatial Discretization was "Least Squares cell based" for gradient and "Second Order Upwind" for momentum, turbulent kinetic energy, turbulent dissipation rate and all other parameters.

3.2.2 Solution Controls

The under –relaxation factors were all set to default values with the Pressure and Momentum under relaxation factors changed to 0.5.

3.2.3 Solution Initialization

- Standard initialization with reference frame relative to zone
- Gauge pressure set to zero
- Velocity components set to zero
- Turbulent kinetic energy(m^2/s^2)and dissipation rate(m^2/s^3) value set to 0.001
- Temperature values set accordingly to the particular parametric study

Chapter 4

Results and Discussion

Post-processing and analyzing the results are the most important parts in a simulation study. ANSYS FLUENT provides very good post-processing options to analyze the results such as the contours of the mass fraction of various species, iso-surfaces which can be clipped to a particular value of a property and many more. This section details the results and their discussions of the three case studies: inert, ideal and non-ideal multicomponent.

In this study, results have been analyzed for Liquid penetration length; vapor penetration length and sauter mean diameter. All the above parameters were plotted against time. Inert case was validated with the experimental results and used a base case for the ideal and non-ideal multicomponent studies. The above mentioned parameters are explained below:

- Liquid Penetration length: Distance travelled by spray droplets before 90% of the droplet mass has been evaporated
- Vapor Penetration length: Distance from the injection point to the point where the species mass fraction is 0.1%
- Sauter mean diameter: Diameter of a sphere possessing the same volume as the particles in a region of study. It represents the diameter distribution in that particular region.

4.1   Inert validation case

The simulation results for liquid penetration length for do-decane have been validated with the experimental data [2]. Validations have been done for three inert cases with different injection parameters and operating conditions as mentioned in

Table 3.4 and 3.5. Fig 4.1 shows the comparison of the liquid penetration length from numerical simulation with the experimental data for different values of B1. Fig 4.2 and 4.3 shows the validation of liquid penetration length for case-2 and case-3(refer Table 3.4 and 3.5). Grid sensitivity studies have been done at varying B1 values and are represented in Fig 4.4. Time sensitivity study has also been done with time steps 1e-04, 1e-05 and 1e-06 for different meshes and is shown in Fig 4.5 and Fig 4.6.
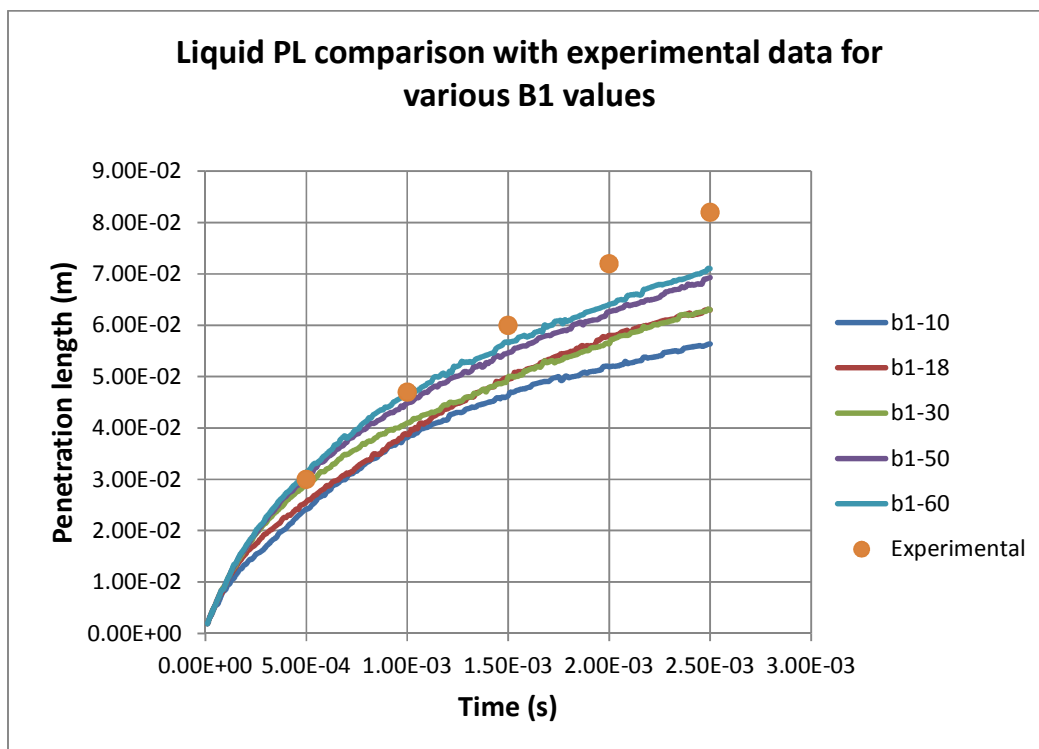
Fig-4.1: Inert Validation for case-1

From the above graph, it can be observed that a value of B1=60 gives minimum deviation from the experimental data up to 1.5e-03. The significant difference in numerical and experimental data in the later time may be due to the error in the experimental measurements as the droplets are too small and dispersed, before they completely evaporate, to be tracked after a particular time for the penetration length.
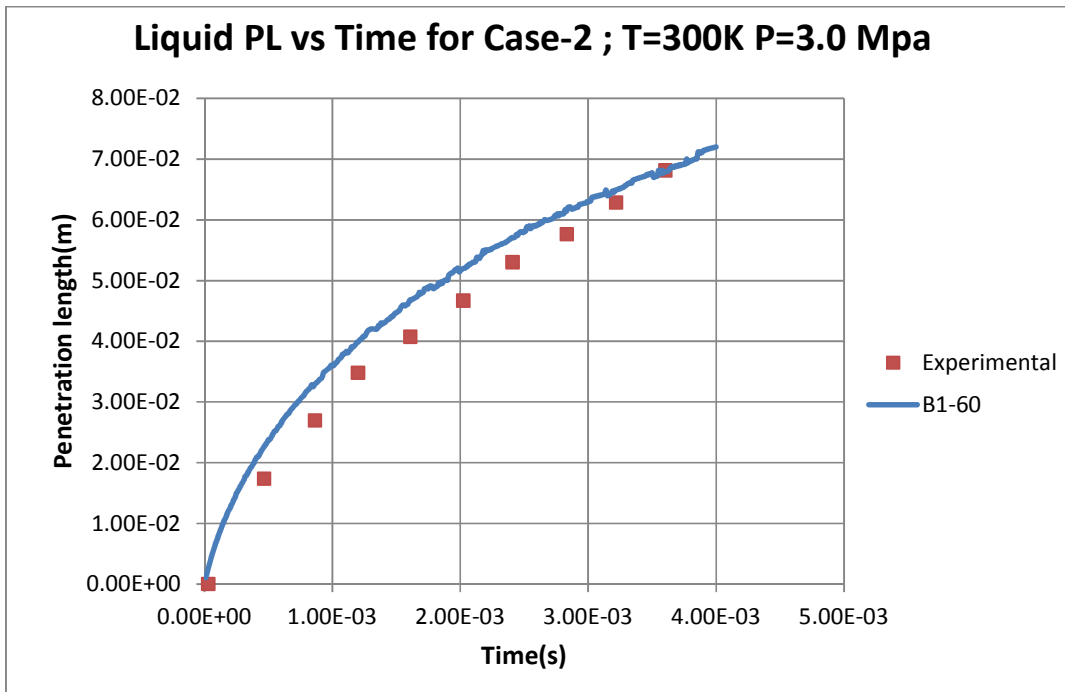
39

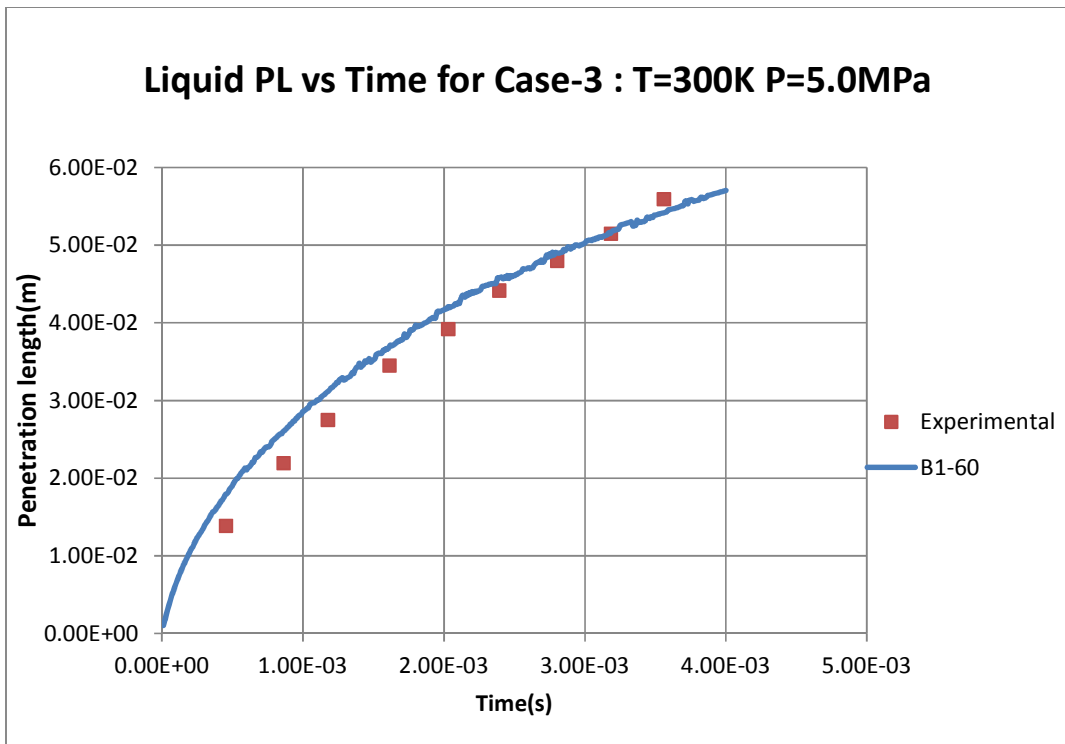**Fig-4.2: Inert validation for case-2**

Fig-4.3: Inert validation for case-3

40

It can be observed from the above plots that the numerical data is comparable with the experimental results for a B1 value of 60. The penetration length was decreased with increased pressures in case-2 and case-3 due to the increased drag force on the droplets and droplets travelling lesser distances.
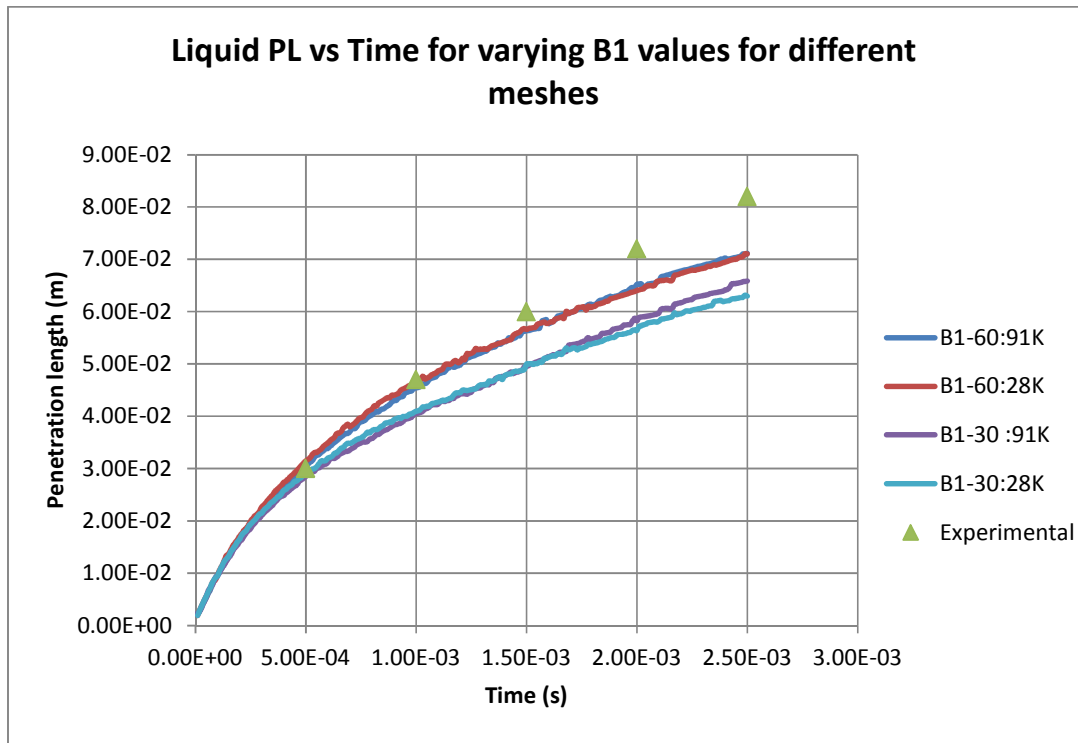

Fig-4.4: Grid sensitivity study for various B1 values

From the grid sensitivity study, it was observed that the inert case was grid independent. Time sensitivity studies showed that the case was time independent for time steps 1e-05 and 1e-06, and giving absurd values for time step of 1e-04. So from the above results, Mesh-3(refer 3.1.1) was selected for ideal and non-ideal multicomponent study with a time step of 1e-05 and B1 =60 as the parameters.

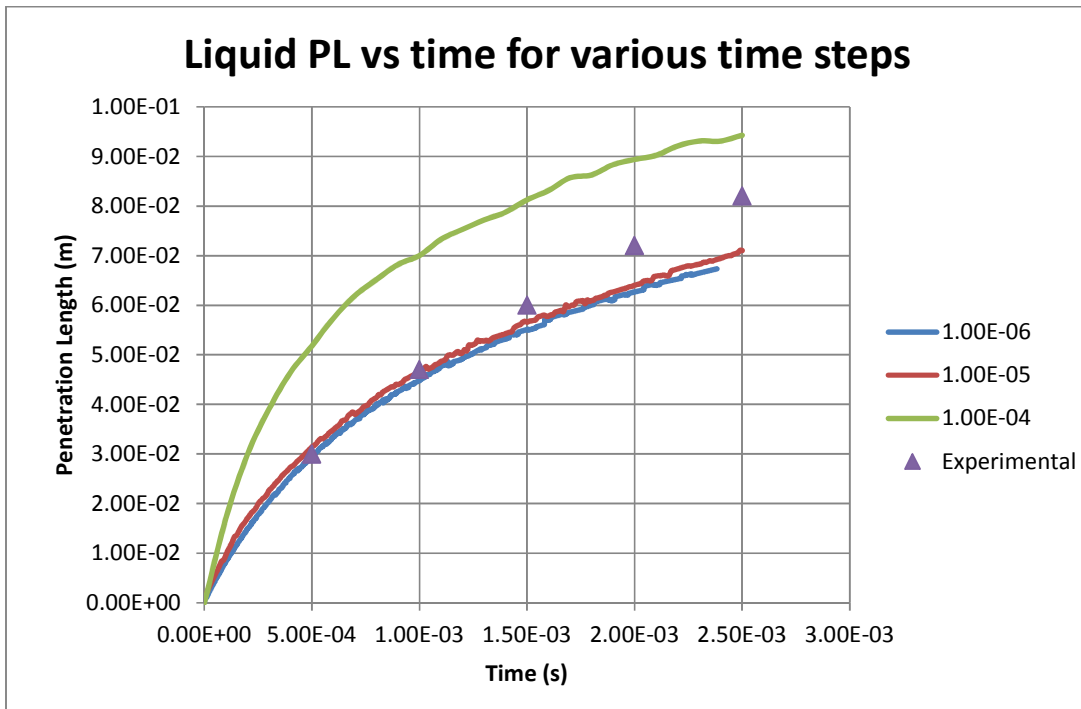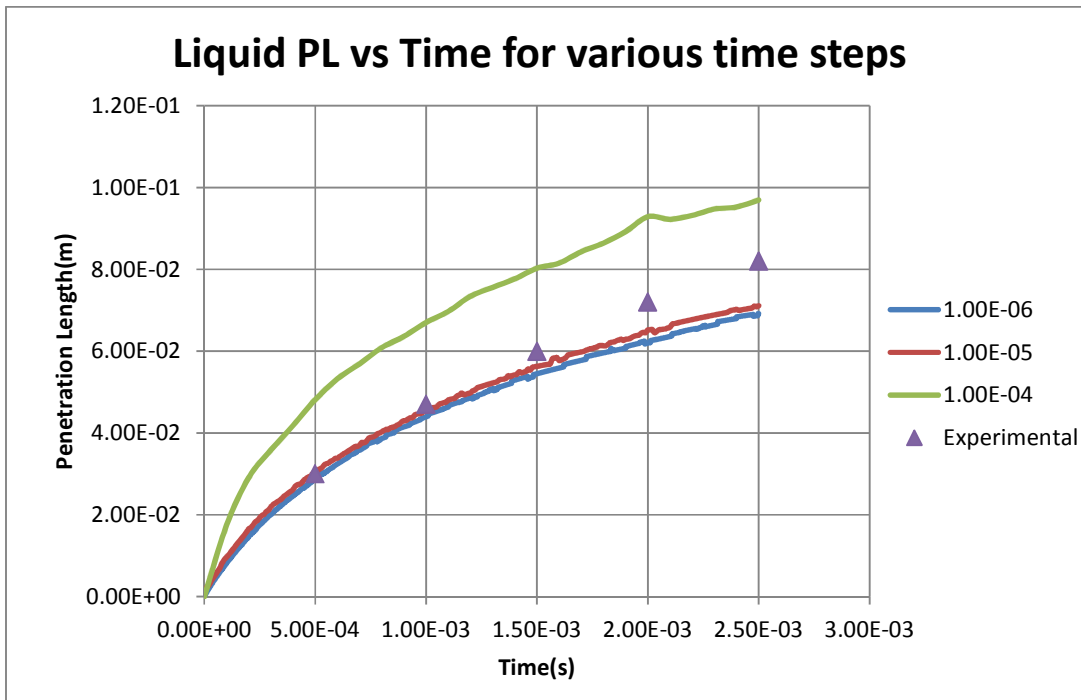Fig-4.5: Time sensitivity study for Mesh-1

Fig-4.6: Time sensitivity study for Mesh-2

4.2   Ideal Multicomponent case

A mixture of is injected in to the chamber for analysis and parametric studies were done on an ideal mixture of iso-octane and nheptane to determine the liquid and vapor penetration depth at various combinations of temperatures and pressures. Sauter mean diameter (SMD) analysis was done in different axial regions of the domain, measured from the injection point. Mole-fraction study was also done to study the effect of concentration of species in the ideal mixture.

Fig 4.7 shows the liquid penetration length comparison for temperatures 500, 700 and 900 K at 1.1 Mpa pressure and half mix of the species in mixture. Fig 4.8 shows the liquid penetration length comparison for pressure 1.1, 3.0 and 5.0 Mpa at 700 K temperature and half mix of the species in mixture. Fig 4.9 shows a mole fraction study at 700 K temperature and 1.1 Mpa pressure for 0-1, 0.5-0.5, and 1-0 mix of species in the mixture. Fig 4.10 shows the vapor penetration length comparison with liquid penetration length for temperatures 500, 700 and 900 K at 1.1 Mpa pressure and half mix of the species in mixture. Fig 4.11 shows the vapor penetration length comparison with liquid penetration length for 1.1, 3.0 and 5.0 Mpa pressures at 700 K temperature and half mix of the species in mixture. Fig 4.12 shows SMD variation with time at various axial locations at 1.1 Mpa pressure and 700 K temperature and half mix of the species in mixture. Fig 4.13 shows SMD variation with axial distance at 1.1 Mpa pressure and 700 K temperature and half mix of the species in mixture for varying time.
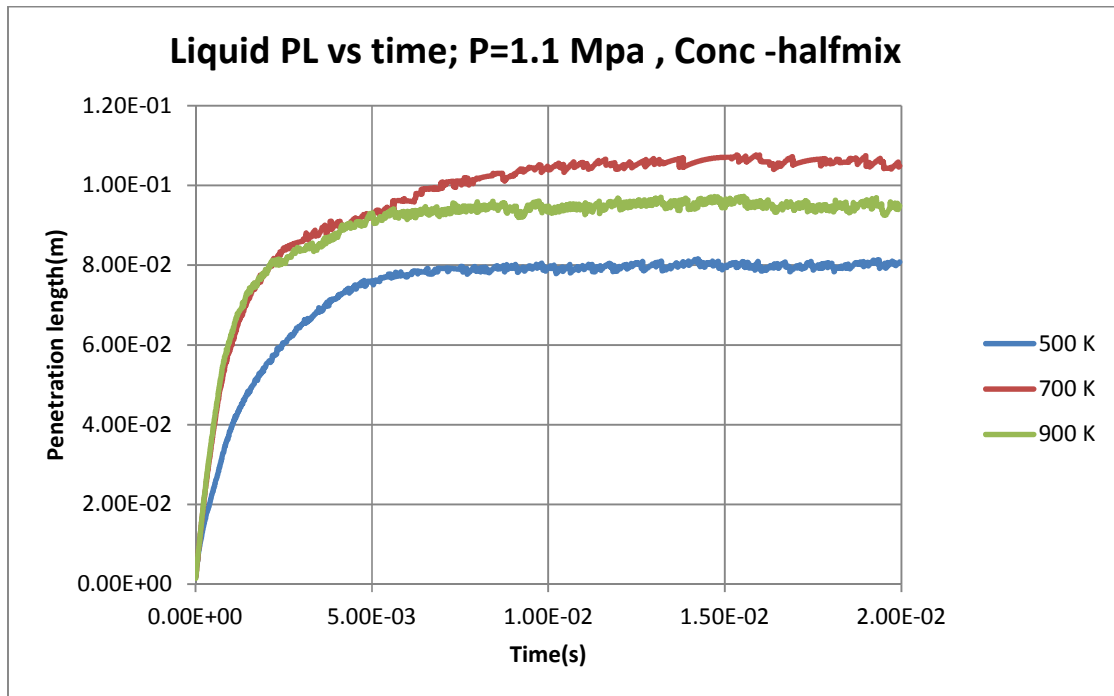
Fig-4.7: Variation of Liquid Penetration length with Temperature

The liquid penetration length depends on a statistical balance between the drag forces on a particle due to the medium and the evaporation rate from the surface of the droplet. As temperature increases the liquid penetration length should decrease as there will be a decrease in the density of medium, but the penetration length was observed to increase with temperature. This may be due to the fact that, the drag forces on the droplet is dominating over the evaporating heat transfer rate from the surface. However the liquid penetration length for 900K was observed to be less than 700K. We can deduce from the above fact that for temperatures 900K and above, the heat transfer rate is dominating over the drag forces and droplets evaporating faster giving a lesser penetration length than 700K. From Fig 4.8, it can be observed that, as the pressure increases the medium becomes denser and the droplets travel lesser distances before they completely evaporate.
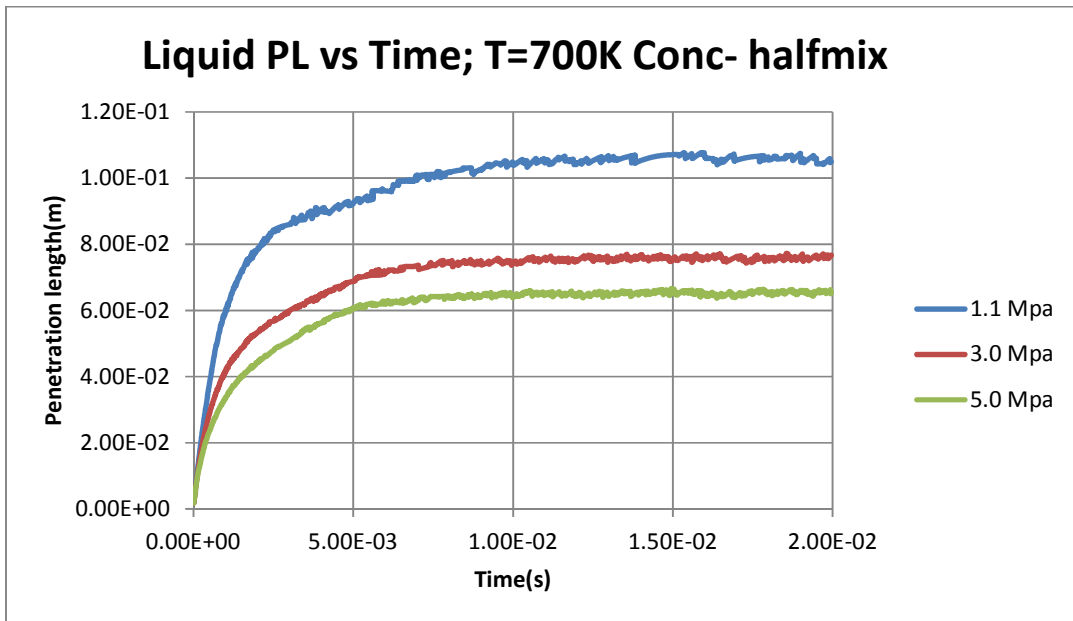
Fig-4.8: Variation of Liquid penetration length with pressures
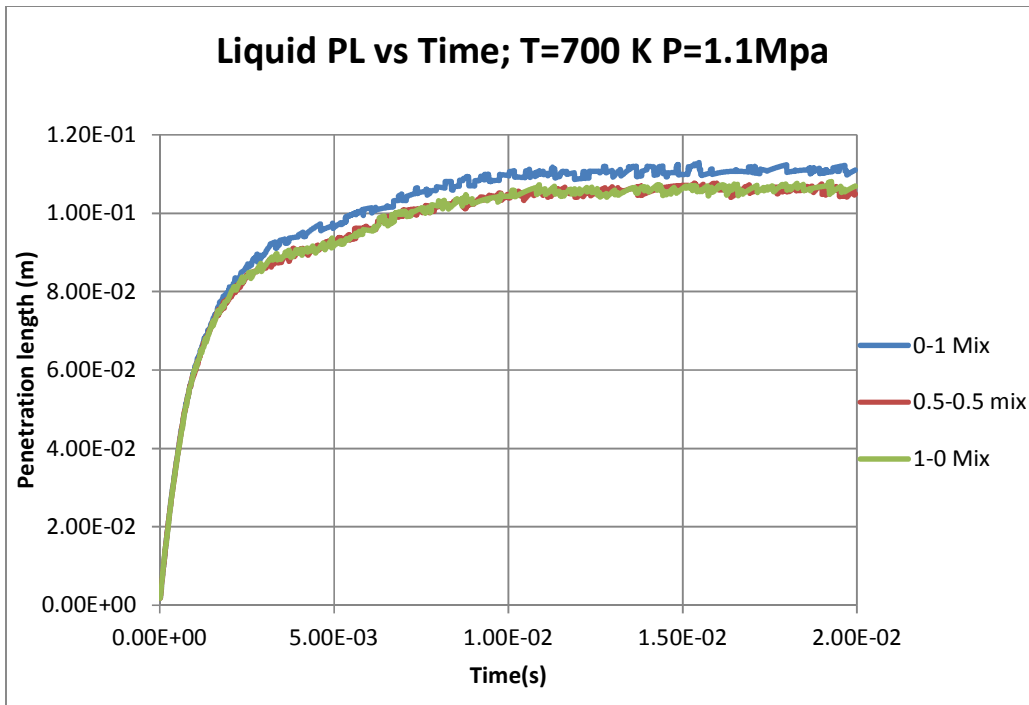

Fig-4.9: Mole fraction study at various mixes of species in mixture

The mole fraction study shows the ideal nature of iso-octane and nheptane as there is no appreciable difference between the penetration lengths for various concentrations of the species in the mixture. However for 0-1 mix, a slightly increase in penetration length is observed. This may be due to the very small variation in the saturation vapor pressures of iso-octane and nheptane.
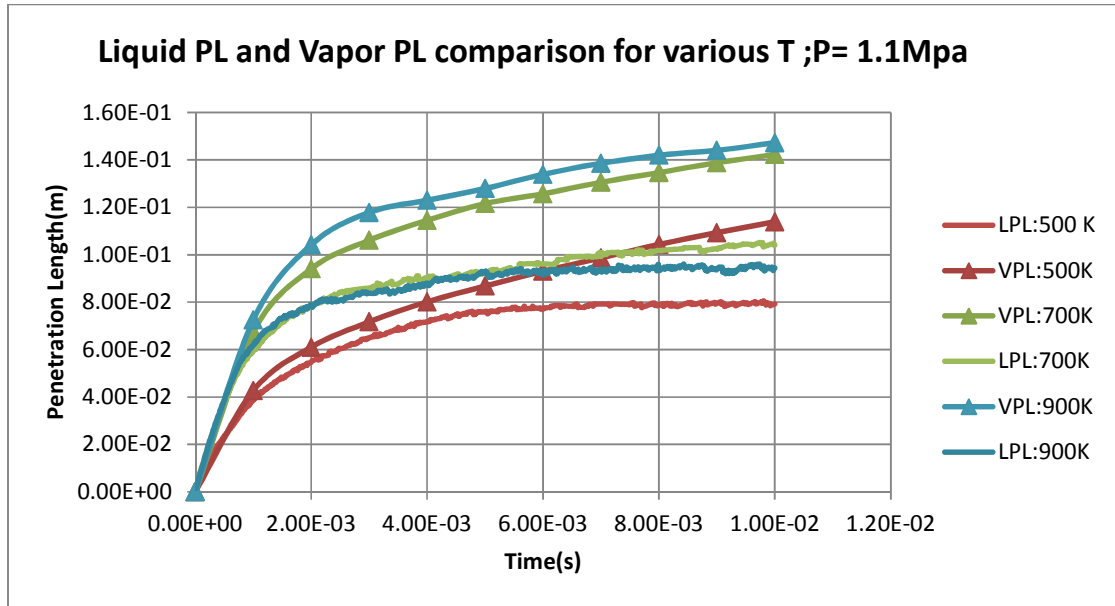

Fig-4.10: Liquid PL and Vapor PL comparison at different temperatures

As we can see from the above graph, the vapor penetration length (lines with markers) is more than the liquid penetration length (normal lines). Vapor PL curve for 900K was observed to be greater than the vapor PL for 700K. This justifies the deduction made earlier for liquid penetration length being lesser for 900K than 700K. This is because the evaporation rate being more for 900K, more amount of vapor will be produced and thus vapor penetration length will be obviously more for 900K. The vapor penetration length was observed to decrease with increased pressures from the Fig 4.11.
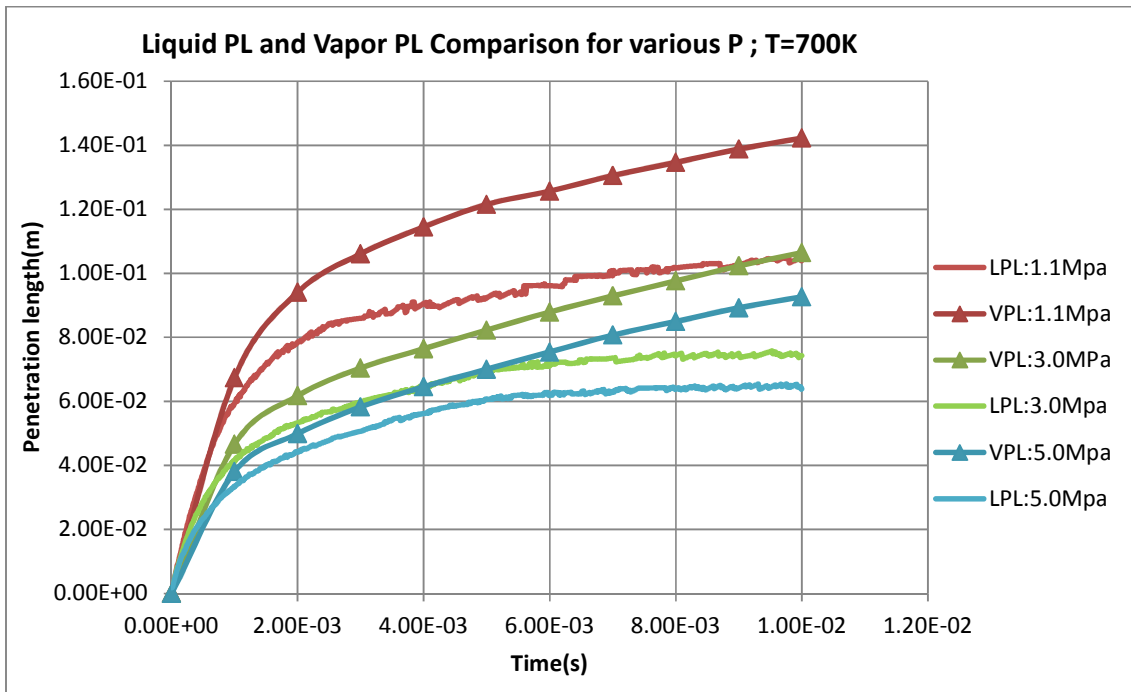
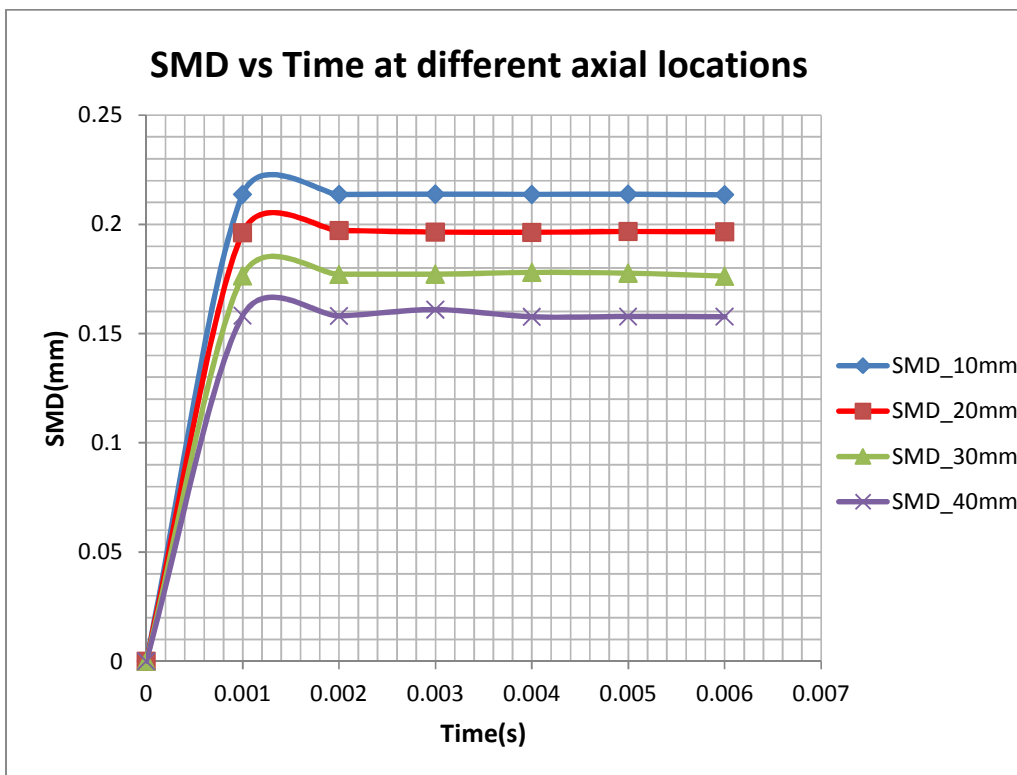Fig-4.11: Liquid PL and Vapor PL for varying pressures

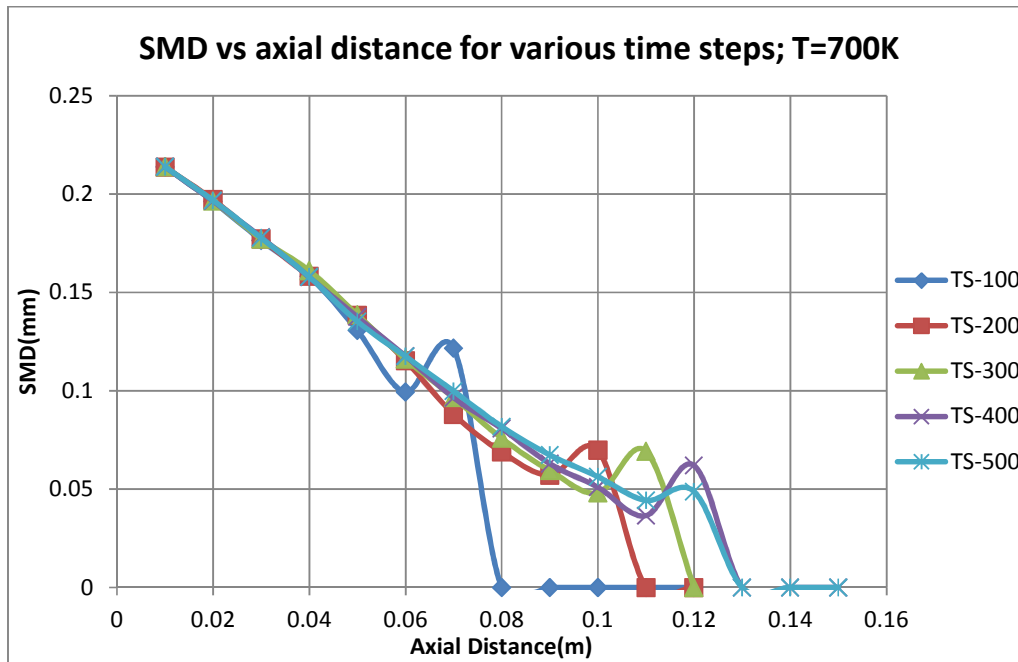Fig-4.12: SMD variation with time for various axial positions

Fig-4.13: SMD variation with axial distance for various time-steps

Fig 4.12 shows the variation of the sauter mean diameter (SMD) with time at various axial distances from the point of injection and Fig 4.13 shows the variation of the sauter mean diameter (SMD) with axial distances from the point of injection at different time for 700K and 1.1Mpa. It is clear from the above graph that the first plane near the injection shows diameters of the droplet comparable to the injection diameter and these droplets break-up into finer ones ultimately the diameter becoming zero(no droplet remain).

4.3   Non-ideal Multicomponent

The simulation studies on the ideal multicomponent mixture are extended to non-ideal multicomponent mixture of iso-octane and ethanol. Parametric studies are done to analyze the vapor and liquid penetration lengths, the effect of temperature and pressure on the mixture, the effects of species concentration on the spray and the sauter mean diameter analysis for predicting the droplet diameter distribution.

48

Fig 4.14 shows the variation of liquid penetration lengths with temperature for a pressure of 1.1Mpa.Fig 4.15 shows the variation of the liquid penetration length with pressure for a temperature of 500K. Fig 4.16 compares the vapor and liquid penetration lengths for varying temperatures at 1.1Mpa pressure. Fig 4.17 shows the variation of SMD with time at various axial distances (10mm and 20mm) from the point of injection.
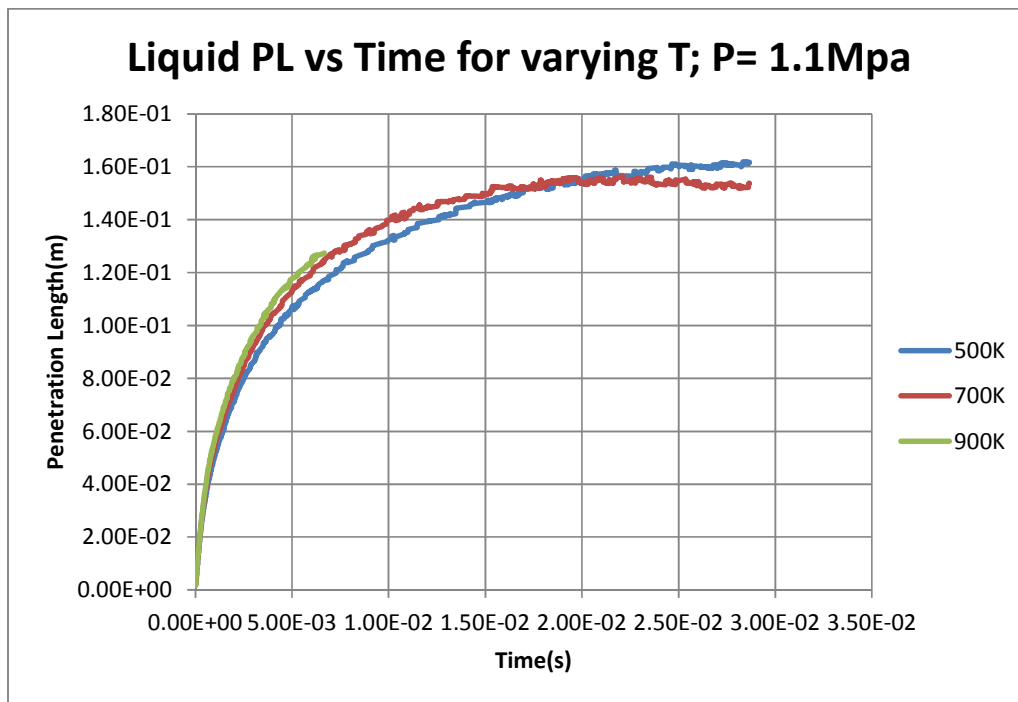

Fig-4.14: Liquid Penetration length variation with temperature

It can be observed from the above graph that, the liquid penetration length is decreasing with increase in temperature. This shows that the evaporation rate is dominating over the drag force part and the droplets evaporate faster at higher temperatures.
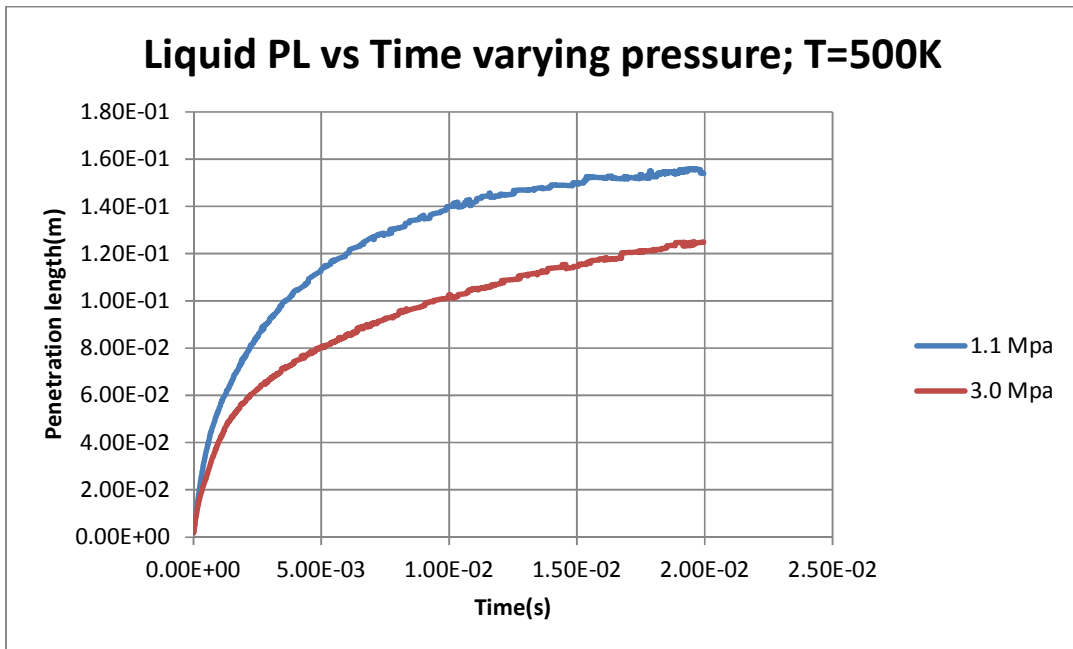
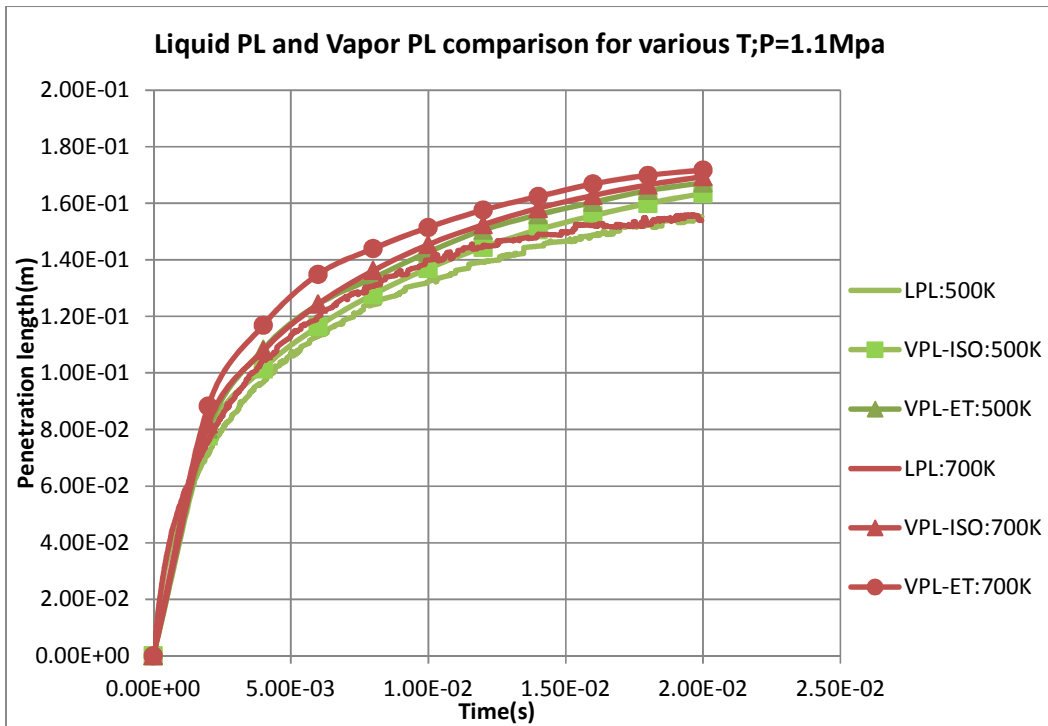Fig-4.15: Liquid penetration length for varying pressures

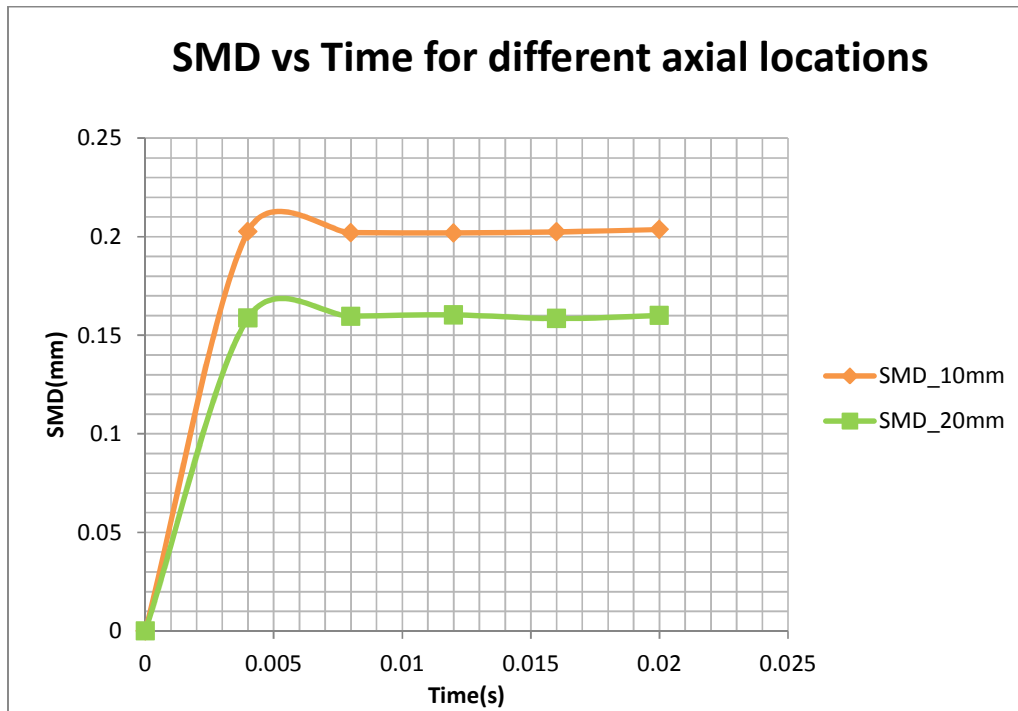Fig-4.16: Liquid PL and Vapor PL comparison for varying temperature

Fig-4.17: SMD variation with time for various axial positions

From Fig 4.15, the liquid penetration length was observed to decrease with increase in pressure, as the medium gets denser. However the change in penetration length for increase in pressures was observed to be at a higher rate than that due to increase in temperature. It can be concluded that operating pressures have a better effect on the liquid penetration length than the operating temperatures inside the chamber. It can be observed from Fig 4.16 that the vapor PL is only little more than the liquid PL. This shows that evaporation rate is less and temperature changes have very little effect on the penetration length. SMD analysis in Fig 4.17 proves that the diameter of the droplets decrease with distance from the injection point due to breakup.

Chapter 5

Conclusion

The study done in this thesis is mainly aimed at developing a robust evaporation model for non-ideal multi component spray mixtures. This study will help in modeling a fuel spray in an IC engine, which in turn helps in achieving a better fuel economy and reducing the emission from the engines. Iso-octane ethanol mixture was chosen for this study. Iso-octane is a reference for the octane rating of the fuel. Ethanol has a high octane number and has very good anti-knocking properties. Ethanol reduces the mission from the engine as it improves the evaporation rate of the mixture. This improves the fuel economy and helps in reducing the cost of fuel. Some of my deductions from this study are stated below.

In inert validation study, it was found that the solution was grid independent for two grid sizes of 1mm and 0.8mm. Time sensitivity studies showed that time steps 1e-05 and 1e-06 provided similar results, but 1e-04 was giving absurd values. It was also observed that for a value of Wave constant B1=60, the simulation results matched the experimental data with minimum error. So the validated base inert case settings were used for the further multicomponent analysis.

The parametric study on iso-octane nheptane mixture showed that, for increasing temperatures, the liquid penetration length was increasing instead on decreasing and it can be concluded that the drag forces on the droplet is dominating over the evaporation rate from the droplet surface. But the liquid

penetration length for 900K was observed to be lesser than that for 700K. It can be concluded that the evaporative mass transfer from the droplet surface is dominating over the drag forces at temperatures of 900K and above. This fact was justified by the plot showing the vapor penetration length for 900K is more than that for 700K. The pressure studies showed an inverse relationship between penetration length and pressure. The mole-fraction studies proved the ideal nature of the mixture as iso-octane and nheptane have comparable saturation vapor pressures and the activity coefficient is one. The vapor penetration depth was observed to be more than liquid penetration length for all parametric studies. The Sauter Mean Diameter analysis showed that the diameter of particles is decreasing with axial distance from the injection, a measure of the secondary break –up.

The simulations study on non-ideal multicomponent mixtures proved to be very complex as the simulation was diverging peculiarly. The divergence was independent of the time step and the under-relaxation factors. The solution was being calculated to give fair results but the solution was seen to be blowing up now and then. A reduction in the wave constant B1 from 60 to 20 made the parametric study more stable and less diverging. Cabin temperatures 500K and 700K were found to give a stable solution than 900K. Iso-octane and ethanol when equally mixed to obtain a 0.5-0.5 concentration mixture was found to be most stable from the mole-fraction parametric studies.

Chapter 6

References

[1] R.Banerjee, "Turbulent conjugate heat and mass transfer from the surface of a binary mixture of ethanol/iso-octane in a countercurrent stratified two-phase flow system", International Journal of Heat and Mass Transfer 51 (2008) 5958–5974, July 2008

[2] Padmesh Mandloi,Jayesh Mutyal, Pravin Rajeshirke elik and Blent zdalyan , "Numerical Spray Calibration Process" , ILASS Americas, 23rd Annual Conference on Liquid Atomization and Spray Systems, Ventura, CA, May 2011,

[3] S. A. Morsi and A. J. Alexander. "An Investigation of Particle Trajectories in Two-Phase Flow Systems". J. Fluid Mech.. 55(2). 193–208. September 26 1972.

[4] J. R. Cash and A. H. Karp. "A variable order Runge-Kutta method for initial value problems with rapidly varying right-hand sides". ACM Transactions on Mathematical Software. 16. 201–222. 1990.

[5] W. E. Ranz and W. R. Marshall, Jr.. "Vaporation from Drops, Part I". Chem. Eng. Prog.. 48(3). 141–146. March 1952.

[6] W. E. Ranz and W. R. Marshall, Jr.. "Evaporation from Drops, Part I and Part II". Chem. Eng. Prog.. 48(4). 173–180. April 1952.

[7] X.Jiang, G.A.Siamas, K.Jagus, T.G. Karayiannis. "Physical modelling and advanced simulations of gas_liquid two-phase jet flows in atomization and sprays" Progress in Energy and Combustion Science 36 (2010) 131_167

[8] Wierzba A , Deformation and Breakup of Liquid Drops in a Gas Stream at Nearly Critical Weber Numbers. Experiments in Fluids , vol 9, pp 5964,(1993)

[9] Reitz RD , Modeling Atomization Processes in High-Pressure Vaporizing Sprays. Atomization and Spray Technology , 3, pp 309337(1987) ,

[10] Reitz RD, Bracco FV, (1986) "Mechanisms of Breakup of Round Liquid Jets" , Enzyclopedia of Fluid Mechanics, Gulf Pub, NJ, 3, pp 233249

[11] P.G. Aleiferis , J. Serras-Pereira , Z. van Romunde , J. Caine , M. Wirth "Mechanisms of spray formation and combustion from a multi-hole injector with E85 and gasoline", Combustion and Flame 157 (2010) 735–756

[12] A. Bader, P. Keller, C. Hasse, "The influence of non-ideal vapor–liquid equilibrium on the evaporation of ethanol/iso-octane droplets", International Journal of Heat and Mass Transfer 64 (2013) 547–558

[13] Peng Zhao, Guoxiu Li, Yusong Yu, "Numerical simulation and experimental study of heat and mass transfer in fuel droplet evaporation", Heat Mass Transfer DOI 10.1007/s00231-014-1317-1

[14] O. Samimi Abianeh, C. P. Chen, "A discrete multicomponent fuel evaporation model with liquid turbulence effects", International Journal of Heat and Mass Transfer 55 (2012) 6897–6907

[15] O. Samimi Abianeh , C.P. Chen , S. Mahalingam, "Numerical modeling of multi-component fuel spray evaporation process', International Journal of Heat and Mass Transfer 69 (2014) 44–53

[16] D.I. Kolaitis, M.A. Founti, "A comparative study of numerical models for Eulerian–Lagrangian simulations of turbulent evaporating sprays", International Journal of Heat and Fluid Flow 27 (2006) 424–435

[17] S.V. Apte, M. Gorokhovski, P. Moin, "LES of atomizing spray with stochastic modeling of secondary breakup", International Journal of Multiphase Flow 29 (2003) 1503–1522

[18] Sergio Hoyas, Antonio Gil, Xandra Margot, Dung Khuong-Anh, Frederic Ravet, "Evaluation of the Eulerian–Lagrangian Spray Atomization
(ELSA) model in spray simulations: 2D cases", Mathematical and Computer Modelling 57 (2013) 1686–1693

[19] Abolfazl Irannejad, Farhad Jaberi, "Large eddy simulation of turbulent spray breakup and evaporation", International Journal of Multiphase Flow 61 (2014) 108–128

[20] M.F. Mohd Yasin, R.S. Cant, C.T. Chong, S. Hochgreb, "Discrete multicomponent model for biodiesel spray combustion simulation", Fuel 126 (2014) 44–54

[21] Santhosh Kumar K, **"**CFD analysis of fuel spray characteristics inside a GDI engine", Indian Institute of Technology, Hyderabad, 2013.

[22] C.S. Lee, R.D. Reitz, Atomization and Sprays 11 (2001) 1–19.

[23] Bruce E. Poling, John M. Prausnitz, John P. O'Connell, "The Properties of Gases and liquids" Fifth Edition

[24] Fluent 13.0 User's Guide, September 2010

[25] Don W Green, Robert H Perry, "Perry's Chemical Engineer's Handbook"